UCRL-16765

University of California
Ernest O. Lawrence Radiation Laboratory

CROSS SECTIONS FOR ELECTRON CAPTURE BY FAST PROTONS IN H_2, He, N_2, Ar

Berkeley, California

DISCLAIMER

UCRL-16765

UNIVERSITY OF CALIFORNIA

Lawrence Radiation Laboratory
Berkeley, California

AEC Contract No. W-7405-eng-48

CROSS SECTIONS FOR ELECTRON CAPTURE BY FAST PROTONS IN H_2, He, N_2, Ar

Leland Merritt Welsh

(Ph. D. Thesis)

August 30, 1966

CROSS SECTIONS FOR ELECTRON CAPTURE BY FAST PROTONS IN H_2, He, N_2, Ar

Contents

CROSS SECTIONS FOR ELECTRON CAPTURE BY FAST PROTONS IN H_2, He, N_2, Ar

Leland Merritt Welsh

Lawrence Radiation Laboratory
University of California
Berkeley, California

August 30, 1966

ABSTRACT

Measurements have been made of cross sections for electron capture by protons, from 440 keV to 13.75 MeV in N_2 and in Ar; to 5.41 MeV in He; and to 2.45 MeV in H_2. These results are presented, along with electron-loss cross sections for the same gases at 1.027 and 2.44 MeV.

The measurements were carried out through analysis of particle beam composition after exit from a gas target of known composition and thickness. The beam was separated magnetically, and the charged and neutral components were detected by Faraday cup and scintillator, respectively.

Our results overlap, between 440 keV and 1 MeV, the experimental results of Barnett and Reynolds. Our σ_{10} cross sections in this region have the same general behavior, but are larger by an amount varying from roughly 10% in hydrogen to 50% in argon.

The results here appear to agree with the prediction of Tuan and Gerjuoy concerning the difference between electron capture by protons in molecular as opposed to atomic hydrogen, although additional measurements will be required to confirm the prediction. There also appears to be a possible correlation between the experimental results in N_2, which show inflections in the capture cross section curve around 1 MeV, and the calculations by Mapleton for capture from that complex atomic system.

There is good agreement between theory and this experiment for the electron-loss cross section.

I. INTRODUCTION

The charge-exchange process investigated in this research is that in which a high-energy proton picks up an electron from an atom, or molecule, of a target gas, thus emerging as a neutral hydrogen atom. Early calculations of cross sections for such reactions did not prove completely satisfactory, and, for that matter, initiated a conflict as to the asymptotic (high energy) behavior of the cross sections which has not yet been completely resolved. There has been a resurgence of interest in the subject, resulting in part from the status of charge exchange as an important loss mechanism in controlled thermonuclear research devices, and interest in its effect upon atmospheric processes. It is also now possible to carry out large-scale numerical calculations which would have been, earlier, totally intractable. Probably this latter ability has contributed most to the proliferation of theoretical work on this problem.

The earliest work of interest was that of Thomas,[1] in 1927, in which he used a purely classical approach to the calculation of capture of an electron from atomic hydrogen by an α particle. The process was viewed as a succession of two Coulomb collisions, first between the α particle and electron, then between the electron and nucleus. The calculation was generally accepted as valid in the high-energy limit, where the de Broglie wavelengths of all the particles involved are much smaller than characteristic atomic dimensions, and gave a result which was proportional to $E^{-11/2}$, i.e., the inverse eleventh power of the α-particle velocity.

The cross section was calculated quantum mechanically in 1930 by Brinkman and Kramers,[2] in the first Born approximation, including in the interaction matrix element only the interaction potential of the atomic electron and the incoming charged particle. This prediction proves to be larger than experimental measurements by about a factor of four at moderately high energies ($\approx$ 100 keV), and generally overestimates experimental results at all energies. In the high-energy limit, this result varies as E^{-6}.

There have been many subsequent refinements to and variations of the quantum mechanical calculation, involving various approximation schemes, some of which are discussed in the section dealing with theoretical development. These have been carried out nonrelativistically, and have usually produced results which in the high energy limit vary either as $E^{-11/2}$ or as E^{-6}. These results have also reduced, in general, the disparity between theory and experimental results.

Experimental results have been available, from several sources, to energies of approximately 100 keV.[3-10] A single set of measurements by Barnett and Reynolds[11] carried the experimental evidence to 1 MeV; above 1 MeV measurements have been limited to isolated points.[12,13]

The work reported here is an effort to extend in a systematic way the energy range of charge exchange measurements for protons in hydrogen, helium, nitrogen, and argon gases. The results presented provide an overlap of previous work down to 440 keV, and extend upward to 13.75 MeV in nitrogen and argon targets.

The energy spread of these measurements is substantial from the standpoint of proton accelerators. Three different accelerators were used in the course of this experiment: a 1-MeV Van de Graaff generator for the lower energies, the Hilac (heavy-ion linear accelerator) of LRL Berkeley, and the 90-inch cyclotron of LRL Livermore for the higher energy points.

The scheme of the measurement is to bring a beam of protons (of known energy) into a gas target (of known composition and density), where some fraction of the protons captures electrons into bound states. Since momentum transfer in this process is negligibly small, the beam of protons and hydrogen atoms exiting the target has the same velocity as on entering. The two components, neutral and charged, of the product beam are then separated magnetically. The neutral particles are counted individually by use of a scintillator-photomultiplier assembly, and the charged component of the beam is collected in a Faraday cup and measured with an integrating electrometer. If the

target gas is "thin" with respect to both the capture and subsequent ionization processes, then the capture cross section, σ_{10}, can be calculated easily from this information.

The details of the experiment are discussed in the body of this report.

II. RESUME OF APPLICABLE THEORY

Many varying approaches to the calculation of the cross section for capture of electrons by fast protons in gases have been made without completely resolving the questions of magnitude or of energy dependence at high energies. Some discussion of the philosophies of these calculations may be found in references 14 and 15, in the review by Bates and McCarroll,[16] and in Mott and Massey.[17] We discuss here calculations which have a more or less direct bearing on our results.

In this discussion, we identify the capturing ion (in most cases a proton) as particle 1, the initial atomic nucleus as particle 2, and the active electron as particle 3. Other particles in the atom will be successively numbered. The great majority of the calculations deal with capture from atomic hydrogen because its simplicity provides a tractable problem.

The differential cross section for electron capture is given by

$$Q(\omega) = \left(\frac{1}{4\pi} \cdot \frac{2\mu}{\hbar^2}\right)^2 \frac{v'}{v} \; |\langle \varphi_f | V_f | \psi_i \rangle|^2, \tag{1}$$

where μ is the reduced mass of the system, v and v' are the beam particle velocities before and after the collision, φ_f is the unperturbed wave function for the final state, and ψ_i is the complete wave function describing the collision.

Finding the exact cross section implies knowing the exact solution of the scattering equation, an integral equation expressed formally as

$$\psi_i = \varphi_i + G_0 V \psi_i, \tag{2}$$

where G_0 is the Green's function operator for the Schroedinger equation without perturbation. The fact that Eq. (2) cannot be solved exactly for this problem gives rise to the many approximations applied to this calculation.

A. Classical Estimate of High Energy Behavior

The classical calculation by Thomas[1] mentioned in the Introduction preceded the wave mechanical attempts, and is interesting for its prediction of high energy behavior. The collision is viewed as a succession of two Coulomb collisions; the sequence of collisions is illustrated in Fig. 1. The first collision is between the atomic electron and the impinging ion, which he took to be an α particle, and results in the electron coming off at 60 deg, the angle at which its velocity has a magnitude U equal to that of the α particle. The electron then scatters off its parent nucleus to align its velocity vector with that of the alpha. Both the electron and nucleus are assumed to have velocities very much smaller than $\vec{V}$, so that they are considered to be initially at rest. This sequence of events is the only one possible, classically, which can lead to a capture under the criterion for capture that the final velocity $\vec{U}$ of the electron must be such that

$$\frac{1}{2} mu^2 \leqslant \frac{2e^2}{a_0} ,$$

where $\vec{u} = \vec{V} - \vec{U}$, and a_0 is the Bohr radius. This calculation leads to a probability of capture with an energy dependence of $E^{-11/2}$.

Cook pointed out,[18] however, that there is no energy region for which this classical calculation can be considered valid. To be valid, the binding energy D of the electron would have to be much greater than the uncertainty in relative energy, ΔE, of the electron and capturing particle, i.e., $D \gg \Delta E$; ΔE in turn is dependent upon the criterion that uncertainty in position must be much less than the impact parameter b of the collision, or $\Delta x \ll b$.

Since $$\Delta x \cdot m\Delta v \geqslant \frac{\hbar}{2}$$

and $$\Delta x \ll b,$$

$$D \gg \Delta E = \frac{1}{2} m(\Delta v)^2 \gg \frac{\hbar^2}{8b^2 m}$$

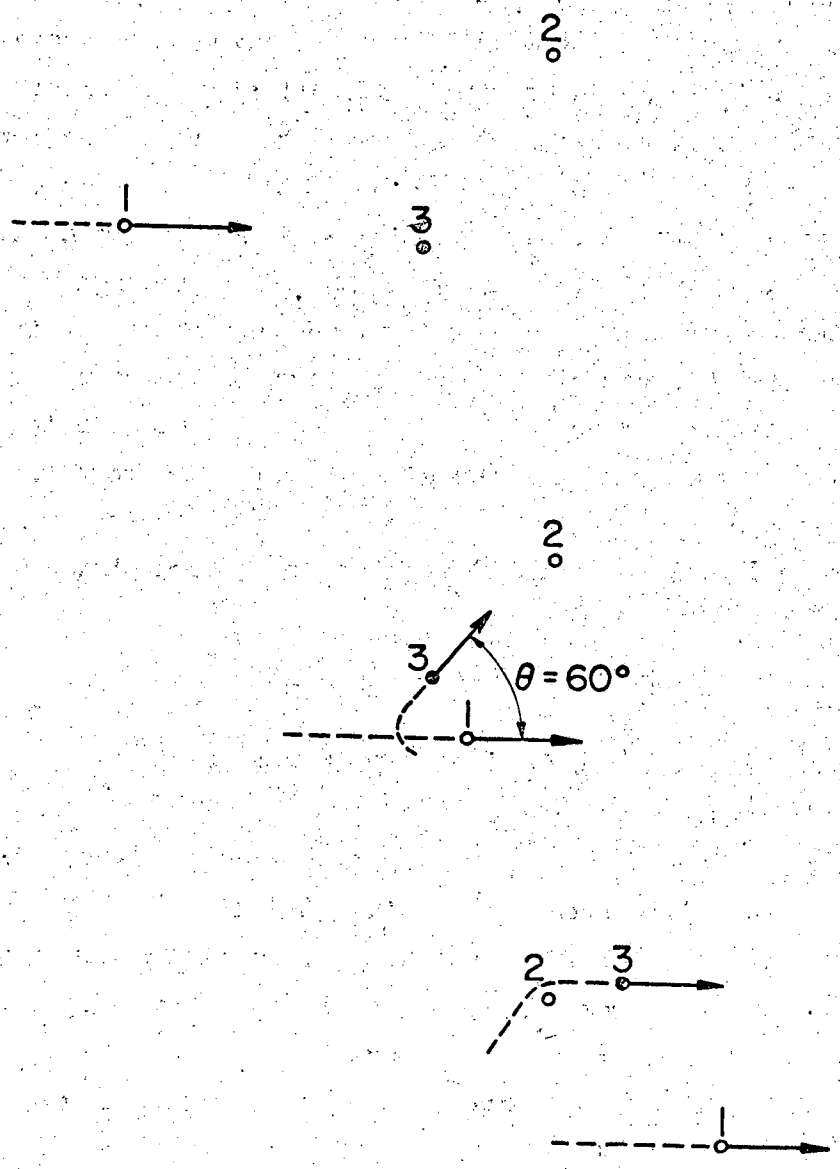

MUB-12367

Fig. 1. Coulomb collisions leading classically to capture of the electron (3) by the impinging ion (1). The parent nucleus is particle (2).

should hold for the calculation to be worthwhile. This inequality is not preserved at high energies, and grows worse as energy rises. We cannot, therefore, consider the classical calculation a weighty argument for expecting an $E^{-11/2}$ dependence at high energy.

More recent efforts to apply classical techniques to the calculation of electron capture have been made by Gryzinski[19] and by Bates and Mapleton.[20] In these cases classical Coulomb collisions are used, but velocity distributions appropriate to quantum mechanical states are imposed upon the electrons. Bates and Mapleton found good agreement with experimental results at low energies, but not in the energy range of the measurements reported here.

B. Born Approximation

Equation (2) is equivalent to

$$\psi_i = \varphi_i + G_0 V \varphi_i + G_0 V G_0 V \varphi_i + \cdots ,$$

which is the Born series. The first Born approximation assumes that $\psi_i \approx \varphi_i$, on the basis that for high energies the interaction potential V is a small perturbation. The first Born matrix element is thus

$$\langle \varphi_f | V_f | \varphi_i \rangle .$$

Successive Born approximations are made by including additional terms of the Born series in the approximate expression for ψ_i.

In 1931, Brinkman and Kramers[2] applied the Born approximation to electron capture by a fast ion, for which the matrix element should be

$$\langle \varphi_f | V_{12} + V_{23} | \varphi_i \rangle .$$

Then, in the manner of Oppenheimer,[21] they chose to ignore, in the interaction potential, $V = V_{12} + V_{23}$, the contribution of the internuclear potential V_{12}, on the physical grounds that this potential gives rise to a small deflection in the path of particle 2, but cannot appreciably affect the probability of electron capture. Therefore

this approximation uses the matrix element $\langle \varphi_f | V_{23} | \varphi_i \rangle$, and is referred to as the Oppenheimer-Brinkman-Kramer (OBK) approximation. Calculation of the OBK cross section for electron capture from atomic hydrogen

$$H^+ + H(1s) \rightarrow H(1s) + H^+,$$

yields a result of

$$Q_{OBK} = \pi a_0^2 \frac{64}{5} \frac{1}{E(1+E)^5},$$

where E is in units of 100 keV.

This E^{-6} behavior at high energy is not changed by the inclusion of the total interaction potential $(V_{12} + V_{23})$ in the calculation of Jackson and Schiff.[22] Their result is

$$Q_{JS} = \left[\frac{1}{192} \left(127 + \frac{14}{E} + \frac{2}{E^2} \right) - \frac{1}{96} \frac{\tan^{-1} E^{1/2}}{E^{1/2}} \left(83 + \frac{15}{E} + \frac{2}{E^2} \right) + \frac{1}{96E} (\tan^{-1} E^{1/2})^2 \left(31 + \frac{8}{E} + \frac{1}{E^2} \right) \right] Q_{OBK},$$

where again E is in units of 100 keV. The asymptotic value of Q_{JS} is 0.661 Q_{OBK}, but this value is approached quite slowly. At 1 MeV the ratio is only 0.369. Surprisingly, from the standpoint of Oppenheimer's argument for the neglect of V_{12}, not only is the effect of the internuclear potential large, but Q_{JS} provides a much better match to experimental results than Q_{OBK} in general.

Higher order calculations have been carried out in the Born series. Drisko found that the second order contribution of the nucleon-nucleon potential cancelled the contribution of the same potential in first order.[23] His second Born result was

$$Q = (0.2946 + 5\pi E^{1/2} 2^{-12}) Q_{OBK}.$$

He estimated that the third Born approximation could have a small contribution falling off as E^{-6}, which begins to raise doubt about the convergence of the Born series for such collisions. Aaron, Amado, and Lee[24] have considered the convergence of the Born series for rearrangement collisions, and produced evidence for the probable divergence of the Born series for rearrangement collisions, independent of the energy E of the incident particle.

The ambiguities presented by the Born approximation in the calculation of cross sections for charge exchange, such as the effect of including the nucleon-nucleon interaction, are rooted in the fact that, since the systems before and after collisions are described by different Hamiltonians, the respective wave functions are generally not orthogonal. Therefore, as it happens, the V_{12} potential has a pronounced effect in the Born approximation even though it can be shown that the effect of the V_{12} term in a calculation involving no approximation, if such were possible, would be of the order of m/M.[25]

C. Further Approximations

Many efforts have been made to develop better approximations to the capture problem and thus eliminate the ambiguities and uncertainties of earlier work. The distorted wave method[26,27] treats the effect of the proton-nucleus interaction by calculating, as a two-body problem, the wave function of the proton in the field of the nucleus. The resultant wave function is then used to represent the incident proton in the initial state wave function ψ_1, as opposed to its plane wave representation in the first Born approximation.

The impulse approximation[14,28,29] further assumes, for high-energy collisions, that the collision time is sufficiently short that the binding of the electron in its original state can be ignored. That is, the collision is considered a two-body collision, between the capturing proton and the electron, where, however, the original state does impose a specific probability distribution of momentum on the electron. Bransden and Cheshire[14] applied this to helium, i.e., for

$$H^+ + He(1s^2) \rightarrow H(1s) + He^+(1s),$$

where the comparison with experiment is made easier by lack of molecular effects. A notable result obtained was a high-energy behavior of $E^{-11/2}$ for capture into the hydrogen ground state.

An energy domain approximating the "high energy" region, where the proton velocity is much larger than the average velocity of the orbital electrons, will be found to occur at lower energies for lighter targets. Generally the capture cross section will fall off with the probability of finding an electron with the velocity v of the incoming proton. The velocity distributions for inner-shell electrons of heavier atoms, which are much more tightly bound, extend much higher than for the electrons of hydrogen or helium.

This behavior of the cross section as a function of the atomic number of the target atom is illustrated in a paper by Mittleman[15] in which he evaluates the capture cross section after considering several forms of the collision matrix element. He produces a first-Born-approximation formula for capture into all s states (capture into other angular momentum states being negligible),

$$Q = a_0^2 \frac{2^{18}}{5} (1.201)\pi^2 \frac{Z}{E^6} n_A(0)\left[1 + 0\frac{Z^2}{E}\right],$$

which he reasons to be valid over the restricted energy ranges represented by

$$10 < \frac{E}{Z^2} < 42,$$

where here E is in units of 25 keV, Z is the atomic number of the atom.[30] In the formula, $n_A(0)$ is the electron density at the origin. The energy limits above are the points between which the E^{-6} term dominates (at the low end) the E^{-7} term of the formula and (at the high end) the $E^{-11/2}$ term of the second Born approximation.

D. Capture from Heavier Atoms

Calculation of electron capture cross sections for complex atomic systems, which is to say for effectively any beyond hydrogen and helium, is difficult and uncertain. The OBK-type calculation can, however, reasonably be done. The suggestion that the ratio Q_{OBK}/Q_{JS} might be close to the same for all atoms at a given impact energy[31] led Mapleton, using that idea, to attempt an estimate of electron capture (hopefully approximating the result of a Jackson-Schiff-type calculation) from atomic nitrogen (and oxygen).[32] To do this, he multiplied his calculated Q_{OBK} for atomic nitrogen by the ratios of the Born cross sections for helium (which he had also calculated[33]) and hydrogen to the OBK cross sections for the same gases, viz.,

$$Q_{JS(est.)}(N) = \frac{Q_{JS}(H)}{Q_{OBK}(H)} \cdot Q_{OBK}(N)$$

and

$$Q_{JS(est.)}(N) = \frac{Q_{JS}(He)}{Q_{OBK}(He)} \cdot Q_{OBK}(N)$$

The respective ratios differ by a maximum of about 40% in the range, 40 keV to 1 MeV, to which he felt it reasonable to apply the method. More interesting, perhaps, from the standpoint of this paper, is the nature of the curve of Q_{OBK}, which Mapleton has now extended to higher energies.[34] It should be pointed out that the curve plotted in Fig. 7 (p. 35) as Ma (2) includes only estimates of capture of p-orbital electrons in atomic nitrogen. At higher energies, capture of 2s and 1s electrons dominates. The curve marked Ma (3) is the OBK result from which Ma (2) was derived, and includes capture of 2p electrons only. Ma (4) includes OBK results for the reactions

$$H^+ + N(^4S;\ 2p^3) \rightarrow H(ns) + N^+(^3P;\ 2p^2) + N^+(^3S;\ 2s\ 2p^3) + N^+(^3S;\ 1s\ 2p^3) + N^+(^5S;\ 1s\ 2p^3).$$

Thus Ma (4) includes all relevant capture reactions, Ma (3) only that of p electrons. The curve for p-orbital capture falls off as E^{-7} at high energy. For capture from s states it falls off as E^{-6}. It appears that the complete Q_{OBK} curve might reproduce approximately the shape, although not the magnitude, of the structure in the experimental curve at around 0.5 to 1 MeV.

E. Comparison with Experiment for Diatomic Gases

It should be noted that a direct comparison of such calculations as those for atomic hydrogen

$$H^+ + H(1s) \rightarrow H(1s) + H^+,$$

with our experiment is difficult. The calculation is for capture into the ground state from atomic hydrogen; the measurement is into all states from molecular hydrogen. A reasonable estimate may be made of the capture into excited states by using Oppenheimer's result[21] that, at high proton impact energies, capture (from the ground state) into s states dominates that into states of higher angular momentum and that capture into a level n is approximately proportional to n^{-3}. Thus capture cross section Q into all states would be

$$Q(1s - nl) = Q(1s - 1s) \sum_{n=1}^{\infty} n^{-3} = 1.201\ Q(1s - 1s).$$

In Figs. 5 (p. 31) and 7 (p.35) the theoretical values for capture from H and N have been multiplied by 2 for comparison with H_2 and N_2 results, despite the fact that Tuan and Gerjuoy have shown such an approximation not to be valid.[35]

The experimental results in hydrogen gas are interesting in that they tend to substantiate the prediction of Tuan and Gerjuoy. Specifically, Tuan and Gerjuoy have calculated $Q_{OBK}(mol)$, the molecular counterpart to the OBK calculation. That is, the calculation is carried out by using molecular orbital wave functions, but again ignoring nucleon-nucleon interactions. At energies somewhat above 400 keV, $Q_{OBK}(mol)$ is less than 2 $Q_{OBK}(atomic)$ as a result of a destructive interference between the capture amplitudes of the two atomic centers. On the other hand, as $v \to \infty$, the interference effect fades and $Q_{OBK}(mol)$ approaches a value between 2.4 and 2.8 $Q_{OBK}(atomic)$, depending on the molecular wave functions used. In molecular hydrogen the electrons are more tightly bound, and therefore have a higher probability of having the velocity v of the capturing proton. The capture amplitude is roughly proportional to that probability. The results plotted in Fig. 5 suggest such behavior when compared with the theoretical values plotted ($2Q_{JS}$).

A consequence of accepting the calculation is that one finds it necessary to go to much higher energies in measurements in H_2 to have any hope of comparing the "asymptotic" behavior at high energy with theory.

Another possible difference exists between calculation and observation. Although the calculations are usually carried out with field-free wave functions, the capturing proton sees a Lorentz field resulting from its high velocity through ambient magnetic fields in the laboratory system. Stray fields at the target are no larger than approximately 1 gauss.

With an estimate of 1 gauss for the magnetic field, one finds the equivalent electric field,

$$\vec{F} = \frac{\vec{v}}{c} \times \vec{B},$$

to be 14 volts/cm at 1 MeV and 52 volts/cm at 13.75 MeV, our maximum energy.

K. Omidvar has calculated[36] the electron capture cross section in hydrogen, using the OBK approximation and parabolic coordinates, appropriate to the case of capture in an electric field. The result of specific interest to us is that the capture cross section for the initial state $n\ n_1\ n_2$ and final state $n'\ n_1'\ n_2'$ is dependent solely on the principal quantum numbers n and n'. The probability of capture into an excited level n is thus independent of the existence of the Lorentz field.

III. APPARATUS AND PROCEDURE

A. General Description

A schematic representation of the experiment is shown in Fig. 2. The beam is accepted in the apparatus at a location as close as conveniently possible to the last bending magnet of the accelerator, a choice intended to minimize the drift path of the beam, thus also the number of neutrals created by exchange with background gas in the drift sections. The calculation of σ_{10} from the data requires a correction term involving σ_{01}, the ionization cross section for the target gas. This need for accurate knowledge of σ_{01} in our energy range led to the inclusion of the neutralizing foil and bending magnet in front of the target section, in order that σ_{01} could also be measured as necessary.

In measuring the capture cross section, σ_{10}, one allows the proton beam to enter the target unimpeded. The charged component of the beam leaving the target is bent by the separating magnet field 10 deg into the Faraday cup used in this case for proton measurement. The neutral component of the beam continues on a straight path into the plastic or cesium iodide scintillator used for detection of neutrals.

In measuring the ionization cross section, one inserts the thin aluminum neutralizing foil in the beam line, then bends away the charged component emerging from the foil with the permanent magnet, thus providing a beam of neutral hydrogen atoms entering the target. In this case, the relative intensities of charged and neutral components entering the detectors are of the same order, so that scintillator techniques are used for measurement of both beams.

The cross sections at each energy are measured at several target pressures. In the σ_{10} measurement, the pressure chosen is such that $\Pi\sigma_{01} < 0.4$, where Π, the target thickness, is the product of target density N (mol/cm^3) and target length L (cm), i.e., $\Pi = NL$ (mol/cm^2). In this way the correction term mentioned earlier is always kept smaller than 20% .

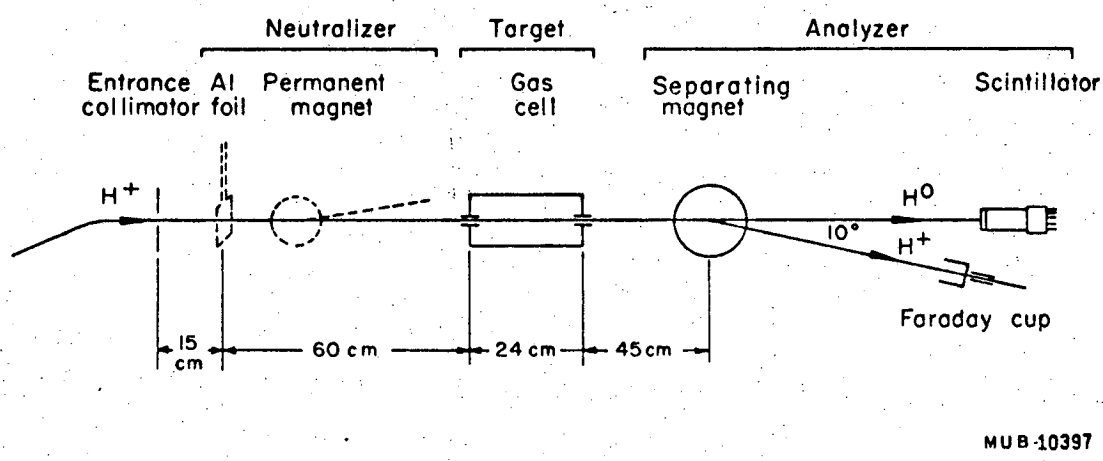

Fig. 2. Schematic of experiment.

B. Detailed Description of Apparatus

Figure 3 is a line sketch, approximately to scale, showing the layout of components in the experiment. Those elements outlined in bold relief in the figure correspond to the basic elements of the experiment shown in the schematic, Fig. 2.

1. Neutralizer

The neutralizer section is used in the course of measuring σ_{01}, the electron loss, or stripping, cross section. Measurements were made of σ_{01} for H_2, He, Ar, and N_2 at 1 and at 2.5 MeV. Measurements had previously been made at this Laboratory at 10 MeV. Since this cross section varies approximately as E^{-1} in this region, sufficiently accurate interpolation is possible. Such measurements required that the beam entering the gas cell be of neutral hydrogen atoms. This neutralization is accomplished by inserting an aluminum foil, of 140 $\mu g/cm^2$ thickness, in the beam line at a position 15 cm behind the 3/8 in. diam entrance collimator. The neutralizer foil is sufficiently thick that the ratio of neutrals to protons reaches an equilibrium value, which is on the order of that for a proton beam emerging from a "thick" gaseous target.[37]

The charged component of the beam is then swept out of the beam line by the field of a permanent magnet placed behind the foil. The 1400-gauss field of the permanent magnet is sufficient to sweep the proton beam completely clear of the entrance collimator (3/16 in. diam) of the gas cell.

2. Target Gas Cell

The gas cell is diagrammed in Fig. 4. The target chamber itself is centrally located in the gas cell assembly, with the differential pumping section extending to both ends. The assembly is pumped by a liquid-nitrogen-trapped 6-in. oil diffusion pump.

Pressures are set in the target chamber by adjustment of the gas inlet flow rate, using a remotely controlled needle valve. Pressures on the order of 100 microns are attainable before the diffusion pump throughput rate becomes excessive.

Pressures in the gas target are measured with a Schulz ion gauge

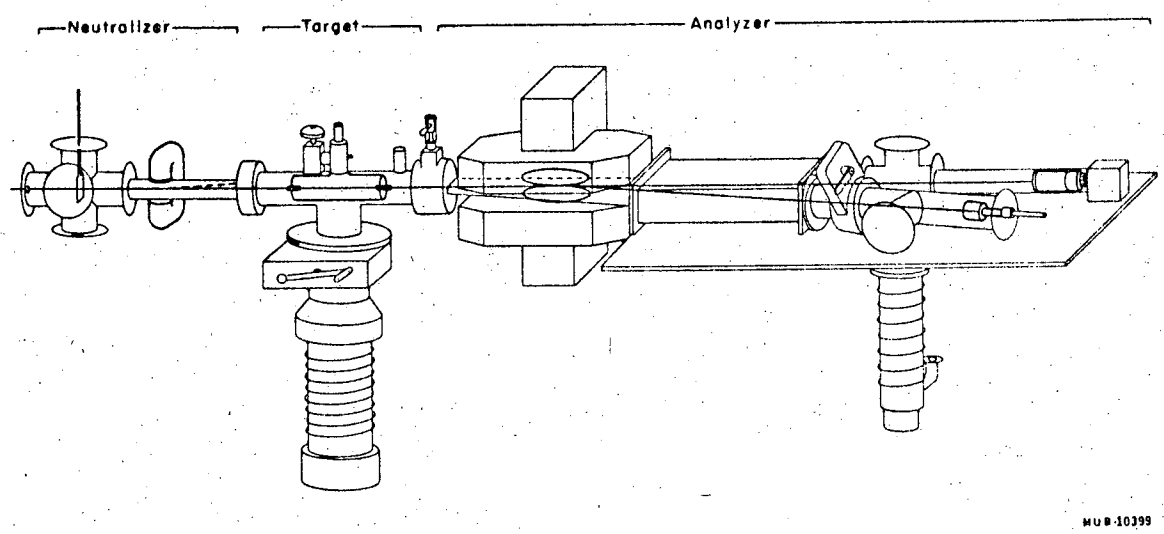

Fig. 3. Line sketch of experiment, approximately to scale. Elements shown in bold relief correspond to the basic elements of the schematic, Fig. 2.

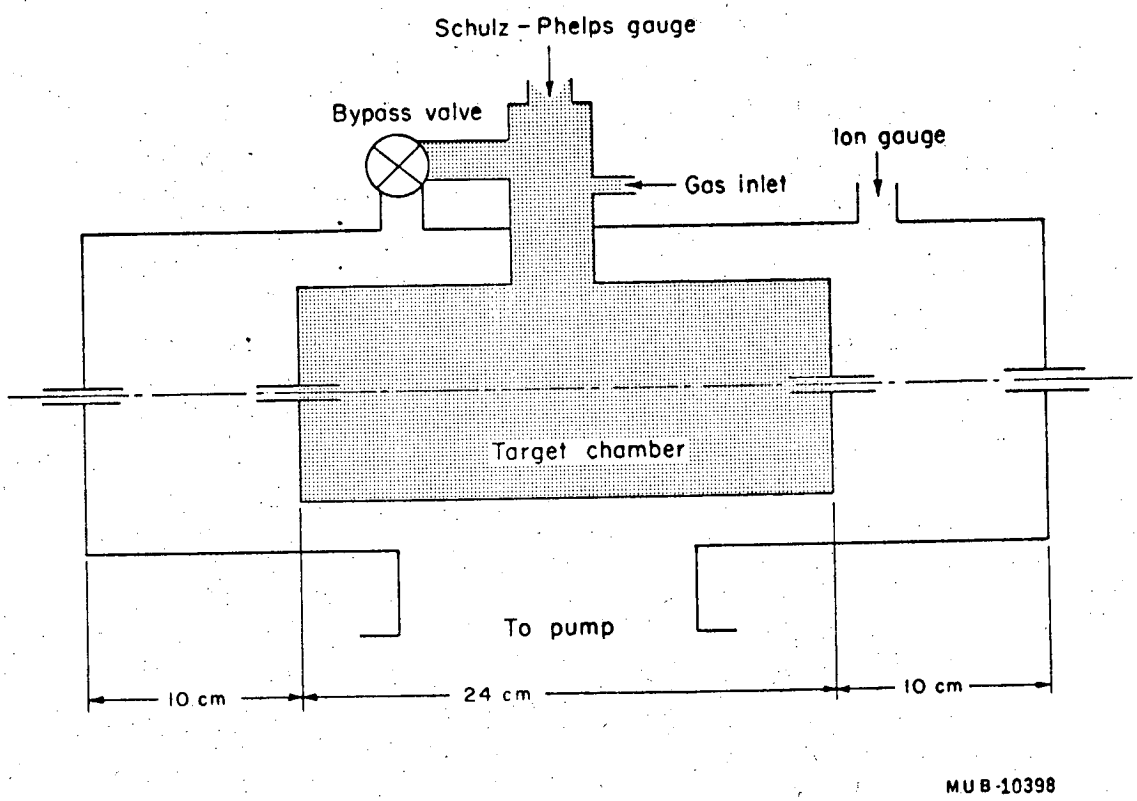

Fig. 4. Gas cell assembly.

tube. The tube is a WL7676, a Westinghouse version of a Schulz-Phelps gauge, designed to operate in the range of 1×10^{-1} to 1×10^{-4} torr. This guage was calibrated, for each of the four gases to be used, against a CVC Model GM100A McLeod gauge. The mercury of the McLeod gauge was cooled to $0^{\circ}C$ in order to avoid the necessity for any corrections due to a pumping effect by mercury vapor flowing toward the cold trap.[38]. The correction is negligible at this mercury temperature.[39]

The random error in pressure calibration was calculated from the variance of the data, with the following results:

Gas	Probable error (%)
H_2	5.1
He	5.0
N_2	5.9
Ar	6.4

Uncertainty in precisely locating the mercury meniscus is the major contributor to error in the McLeod gauge. There is a random error in reading the gauge which is dependent to some extent upon operator skill, and there is an error from variation in the capillary depression of the mercury column which is a function of the condition of the capillary wall surface.[40]

Estimating the capillary depression error to be of approximately the same size as the random errors, we expect a standard error in pressure measurement very slightly less than 10%.

The target chamber collimating tubes are 3/16 in. in inner diameter, are both 4.4 cm long, and are separated by a center-to-center distance along the beam line of 24.4 cm.* The pressure in the

*Subsequent to taking data at the 90-inch cyclotron (Livermore), small modifications were made to the gas cell in which the distance mentioned changed from 24.3 to 24.4 cm, and the i.d. of the entrance collimator to the assembly was reduced from 1/4 in. to 3/16 in.

collimator tubes of the target chamber is assumed to fall off linearly; this makes the effective length of the chamber equal to the center-to-center distance mentioned above. During operation, the pressure in the pumping section remained less than 0.5% of the pressure in the target chamber. Thus the pumping section made no significant contribution to the effective target thickness.

3. Analysis Section

(a) Separating magnet and drift sections

The magnet used for beam separation following the gas cell has pole faces 8 in. in diameter, with a gap separation of 2 in. This magnet bends the proton beam 10 deg at a position 45 cm after the exit of the target chamber. The maximum magnetic field required (for 13.75 MeV protons) is 4650 gauss. Measurements of the field strength of this magnet made along a radius indicate that the stray field at the nearest point of the target chamber (the exit) is less than 10^{-4} of the central field, which is to say on the order of the earth's field or less.

The drift sections, both before and after the gas cell assembly, are pumped by liquid-nitrogen-trapped 4-in. oil diffusion pumps. Base pressures are approximately 4×10^{-6} torr in these sections.

(b) Faraday cup

During measurement of the electron capture cross section, the magnitude of the charged (proton) beam is always larger than that of the neutral beam by at least a factor of 10^3. We are thus able to monitor the charged beam with Faraday cup and electrometer while counting the neutral beam with a system of scintillation counter, amplifier, and scalers.

The Faraday cup is 1.75 in. i.d., and is 1.5 in. deep. The problem of losing the secondary electrons emitted when the beam strikes the surface of the cup is overcome by placing a pair of semicircular permanent magnets, 4 in. i.d., with like poles butted together, around the Faraday cup. These magnets produce an average 500-gauss field perpendicular to the beam line, which is sufficient to confine the

secondaries to the cup. The magnets are 4 in. wide, so that their field includes the entire volume of the Faraday cup.

The current collected by the Faraday cup is measured with an LRL integrating electrometer, measuring the voltage rise on a capacitor of known value as charge is collected. The system utilizes a feedback amplifier in order to maintain the cup potential at ground, independent of the charge collected. Calibration is accomplished with a battery-and-precision-resistor current source which is independently calibrated with a Keithley 401 electrometer. We estimate the uncertainty in knowledge of proton beam magnitude as ± 1.5%. The integrating electrometer is used to gate off the scalers counting the neutral beam when some appropriate preset charge level is reached.

(c) Scintillator and photomultiplier assemblies

Two varieties of scintillator-photomultiplier assembly have been used in the course of this work. They differ in the type of scintillator material used and in the type of photomultiplier rather than in any fundamental way.

At the higher energies, 2.45 eV and above, a plastic scintillator of 1.5-in. diameter and nominal 1/32-in. thickness is mounted onto a Lucite light pipe, which is in turn mounted to the face of a type RCA 6810A photomultiplier tube. The light pipe is present to provide a physical separation between the phototube and the magnets associated with the Faraday cup. The tube is further protected from stray magnetic fields by a cylindrical mu-metal shield around the tube and a soft-iron shield around that.

At energies of 1 MeV and below, a cesium iodide scintillator is used, giving substantially greater light output. This scintillator is mounted directly onto a type RCA 6655A photomultiplier tube. Here also the scintillator has a diameter of 1.5 in. The tube is shielded by an arrangement of mu-metal and soft-iron shields similar to that of the other assembly.

The output of the photomultiplier is amplified, and the pulses counted by scalers, after the discrimination of low-level noise. The

pulses produced by beam particles are monochromatic, and are significantly larger than those of the noise. Thus it is easy to discriminate between noise and true counts.

The choice of detector size (1.5 in. diam) was governed by the need to capture essentially all the particles in the respective beams. As we have mentioned earlier, the momentum transfer associated with the electron capture reaction is small. The magnitude of the scattering angle has been calculated[14,22,26] and has been investigated experimentally, although not to energies as high as for this work.[41] The experimental work extended to 55 keV, measuring the half-angle, $\theta/2$; the significance of this angle is that 50% of the scattered particles emerge within a cone of central angle θ. The results are summarized as follows: The half-angle is a decreasing function of beam energy, down to an apparent minimum which depends on the molecular size and the "thickness" of the target gas, and which is of the order of 1 milliradian.

Calculations of the angular scattering predict a characteristic scattering angle also of the order of 1 milliradian. Typical of these is the calculation by Bransden and Cheshire[14] for 222-keV protons in a helium target showing the usual peaking in the forward direction with a characteristic angle of scattering of less than 0.4 milliradian. One milliradian corresponds to a displacement at the detector of $\approx$0.07 in.

Calculations also point qualitatively to an explanation for the unexpected "minimum" scattering angle. The probability of electron capture, expressed as a function of impact parameter, peaks at smaller and smaller impact parameters for larger and larger energies.[26,42] Of course, the momentum exchange between proton and nucleus is larger at smaller impact parameters.

Some neutral hydrogen atoms formed in exchange collisions near the outer edge of the beam may be scattered so as to fail to pass through the exit collimator. For the particular operating geometry used, we estimate this loss of neutrals to be no more than approximately 1% of the total neutral beam.

The 1.5-in. detector size was chosen as a conservative size, i.e., one more than large enough to serve satisfactorily. The neutral beam was observed visually, by means of a phosphor plate, to be less than 0.75 in. in diameter. Measurements on nitrogen, at 1 MeV, were duplicated with detectors of 1 in. and 1.5 in. diameter, and were found to be the same within statistical errors in counting.

C. Energy Measurement

The very strong energy dependence of the capture cross section demands that the proton beam energy be accurately determined. Three means (listed below) have been used to determine the energy of the proton beams in the course of these measurements. At all energies, and therefore on all three accelerators, energy measurements have been made with a solid state detector. The 90-inch cyclotron includes a system of aluminum attenuating foils and counters (called a "ranger") which was used during measurements at 2.5, 4.8, and 13.8 MeV. Energy calibration of the 1 MeV Van de Graaff further includes the use of proton nuclear resonance capture reactions in lithium and fluorine.

1. The solid state detector used is a lithium-drifted silicon crystal with a maximum depletion depth of 3 mm. This active depth is sufficient for the full-energy beam of the cyclotron, the maximum encountered in these investigations. The pulse produced in the detector with each particle entering is directly proportional to the energy of the particle. The pulse output of the detector, suitably amplified, is fed into a pulse height analyzer (PHA). This is done also with the output resulting from exposure to Am^{241}, a source of 5.477 MeV α particles. By further using the 5.477-MeV alphas attenuated to a known energy by passage through a 0.5-mg/cm^2 aluminum foil, one establishes the energy separation per PHA channel. This information allows a determination of beam energy which is accurate under normal circumstances to ± 1%.

2. The cyclotron "ranger" acts by scattering a small fraction of the primary beam in a tantalum foil set at 45 deg to the beam line. Collimators select particles scattered at 90 deg in such a way that

they exit from the back side of the scattering foil. These particles pass through a system of attenuating foils, then into two in-line proportional counters operating in anticoincidence. The beam energy is derived from a knowledge of the attenuator thickness necessary to slow down the particles sufficiently that they stop in the thin window between the counters (more accurately, either in the window or in the near one-half of either of the two counters). This device is also expected, under good conditions, to give an energy measurement accurate to ± 1%.[43]

3. The primary energy determination for points taken on the 1 MeV machine has been made from certain resonance reactions occurring with protons in lithium fluoride. These are listed as:[44]

Reaction	Energy (keV)	Half-width, Γ (keV)
$F^{19}(p, \alpha\gamma)O^{16}$	872.5	4.5
$F^{19}(p, \alpha\gamma)O^{16}$	340.5	2.7
$Li^{7}(p, \gamma)Be^{8}$	441.2	12.2

These reactions were used to calibrate the magnetic field monitor of the bending (selecting) magnet located just before the entrance to the apparatus. The reactions were detected in two different targets, one a thin layer of LiF deposited on a Lucite plate, the other a thin piece of Teflon (CF_4). The targets were mounted at the end of the neutral beam port in the analysis section, and so used a fully collimated beam. The detector used was a 2-in. diameter, 2-in. thick sodium iodide scintillator, with a type RCA 6655A photomultiplier tube. This assembly, detecting the gammas emitted, was placed against the back side of the target mounting plates. It subtended perhaps a quarter of the total solid angle.

One should note that in the measurement of the stripping cross section, σ_{01}, the energy of the beam has been attenuated by the 140 $\mu g/cm^2$ neutralizing foil. This attenuation is estimated, by use of calculated values of -dE/dx for aluminum,[45] to be ≈ 0.028 MeV at 1 MeV and ≈ 0.013 MeV at 2.5 MeV.

IV. ANALYSIS OF DATA

A. Calculation of σ_{10}

The calculation of the capture cross section is facilitated by the fact that we have a two-component beam, consisting only of H^+ and H^0. The attachment cross sections, for the formation of H^-, are negligibly small at these energies.[46] The gas target is always "thin" with respect to the capture reaction; that is, the mean free path for the capture reaction is very much larger than the target length.

Defining $n_0 \equiv$ density of neutrals (H^0) in the beam,

$n_+ \equiv$ density of protons (H^+) in the beam,

and $n_0 + n_+ = n \equiv$ total density of beam particles,

we find the appropriate rate equation to be

$$\frac{dn_0}{d\pi} = n_+\sigma_{10} - n_0\sigma_{01} ,$$

where $d\pi = Ndx$ and $N \equiv$ target gas density. That this analysis is done for the "thin" target case means that $n_+ \gg n_0$, or alternatively, $n \approx n_+$. In the course of the measurements, $n_0 < 10^{-3}\, n_+$ at all times; for that matter, in all but a few cases $n_0 < 2 \times 10^{-4}\, n_+$. As a reasonable approximation, therefore, we write

$$\frac{dn_0}{d\pi} = n\sigma_{10} - n_0\sigma_{01} ,$$

$$\int_{n_{bl}}^{n_0} \frac{dn_0}{n_0 - n(\sigma_{10}/\sigma_{01})} = -\sigma_{01}\int_0^{\pi} d\pi = -\sigma_{01}\int_0^{L} N\, dx ,$$

where n_{bl} is the background neutral density entering the target chamber. This equations gives, as a solution for σ_{10},

$$\sigma_{10} = \frac{(n_0 - n_{b1}e^{-\Pi\sigma_{01}})\sigma_{01}}{n(1 - e^{-\Pi\sigma_{01}})} .$$

Note that the n_0 of this formula is the neutral density at the exit of the target chamber. The density, N_0, measured at the detector will be increased by the contribution, n_{b2}, of exchanges taking place between the chamber exit and the separating magnet.

Thus, finally,

$$\sigma_{10} = \frac{(N_0 - n_{b2} - n_{b1}e^{-\Pi\sigma_{01}})\sigma_{01}}{N_+(1 - e^{-\Pi\sigma_{01}})} .$$

To account completely for the effect of the neutral background, one needs to know the relative contributions of n_{b1} and n_{b2} to the total measured neutral background count, n_{b0}. The experiment as constructed is not capable of separating these contributions, so that they must be estimated from a knowledge of their sources.

The majority of the background neutrals can be accounted for by a calculation of the number of exchanges expected, at the observed drift section pressures, in a background gas of N_2. Some contribution is also made by scraping collisions of beam particles on the various collimators of the gas cell assembly. From these considerations, plus the relative lengths of drift section before and after the gas cell, we estimate that $n_{b1} \approx 0.8\ n_{b0}$ and that $n_{b2} \approx 0.2\ n_{b0}$. The effect of the uncertainty of this estimate upon the error of the cross section measurement is discussed in the presentation of results.

Chemical analysis of the target gases showed significant impurities to be present only in the hydrogen source bottle. Nitrogen, CO_2, and CO were found to the extent of 0.02, 0.004, and 0.015%, respectively. These small concentrations are significant because their respective capture cross sections are larger than that of hydrogen gas by a factor of some 50 to 800 through our range of energies. Correction for the presence of these impurities is made by subtracting,

from the total measured capture cross section, that amount attributable to the impurities. The total σ_{10}, measured in units of cm^2 per molecule of target gas (H_2), is

$$\sigma_{10}\ (\text{total}) = \sigma_{10}\ (H_2) + \sum_j g_j \sigma_{10}(j)$$

where g_j is the concentration (molecules/molecule of H_2) of impurity j. The effect is larger at higher energies. Estimates of the CO_2 and CO cross sections were made on the basis of the meager experimental evidence available.[6] We are aware of no theoretical work directly applicable. The effect of this uncertainty upon the σ_{10} standard error is also discussed.

Measurements have been made, for each target gas and beam energy, at several target pressures. The cross section is calculated for each measurement individually. The result quoted for a given gas and energy is the average of these measurements, which are typically ten in number.

B. Calculation of σ_{01}

Since this measurement utilizes a beam of H^0 entering the target, and since $\sigma_{01} \gg \sigma_{10}$ throughout the range of our interest, the rate equation

$$\frac{dn_+}{d\pi} = n_0\sigma_{01} - n_+\sigma_{10} = -\frac{dn_0}{d\pi}$$

simplifies to

$$\frac{dn_+}{d\pi} = n_0\sigma_{01} = -\frac{dn_0}{d\pi};$$

$$\int_n^{N_0} \frac{dn_0}{n_0} = -\sigma_{01}\int_0^{\Pi} d\pi$$

has the solution

$$\sigma_{01} = \frac{1}{\Pi} \ln \left[1 + \frac{N_+ - n_{b+}}{N_0} \right]$$

In this instance, the source of background protons, n_{b+}, is of no consequence.

As before, the result quoted for a particular target gas and H^0 beam energy is an average of the values calculated from approximately 10 measurements made at various target pressures.

V. EXPERIMENTAL RESULTS

A. Tabulation of Cross Sections

The results of the measurements of σ_{10}, the electron capture cross section, and σ_{01}, the electron loss cross section, are presented below for each of the target gases.

1. Hydrogen Gas, H_2

σ_{10} (cm^2/mol)	Proton energy (MeV)
$3.5^6 \pm 0.3 \times 10^{-20}$	0.440 ± 0.003
$4.0^2 \pm 0.5 \times 10^{-21}$	0.654 ± 0.003
$1.1^3 \pm 0.1 \times 10^{-21}$	0.851 ± 0.004
$3.4^6 \pm 0.4 \times 10^{-22}$	1.063 ± 0.006
$5.9^7 \pm 1.3 \times 10^{-24}$	2.45 ± 0.03

σ_{01} (cm^2/mol)	H^0 energy (MeV)
$2.1^5 \pm 0.2 \times 10^{-17}$	1.027 ± 0.006
$8.5^2 \pm 0.8 \times 10^{-18}$	2.44 ± 0.03

These results are plotted in Fig. 5, with other available experimental results. Present results are shown as solid vertical bars, the height being approximately the associated error (the scale of the figures precludes exactness). The straight dashed line through the σ_{10} data has a behavior of $\sim E^{-5.1}$. An accurate determination of the slope demands a much more accurate knowledge of proton energy than of the measured cross section, because of the strong energy dependence of the σ_{10} curve. From the uncertainties in E and σ_{10}, we assign an uncertainty in the exponent of ± 0.15, i.e., σ_{10} varies as $E^{-5.1 \pm 0.15}$. The present σ_{10} results, considered either alone or in conjunction with Barnett and Reynolds results, show no tendency toward a greater slope with increasing energy. The Jackson and Schiff Born-approximation calculation[22] is shown as a typical calculation for comparison purposes. The Jackson-Schiff result reaches an E^{-6} behavior at higher energies.

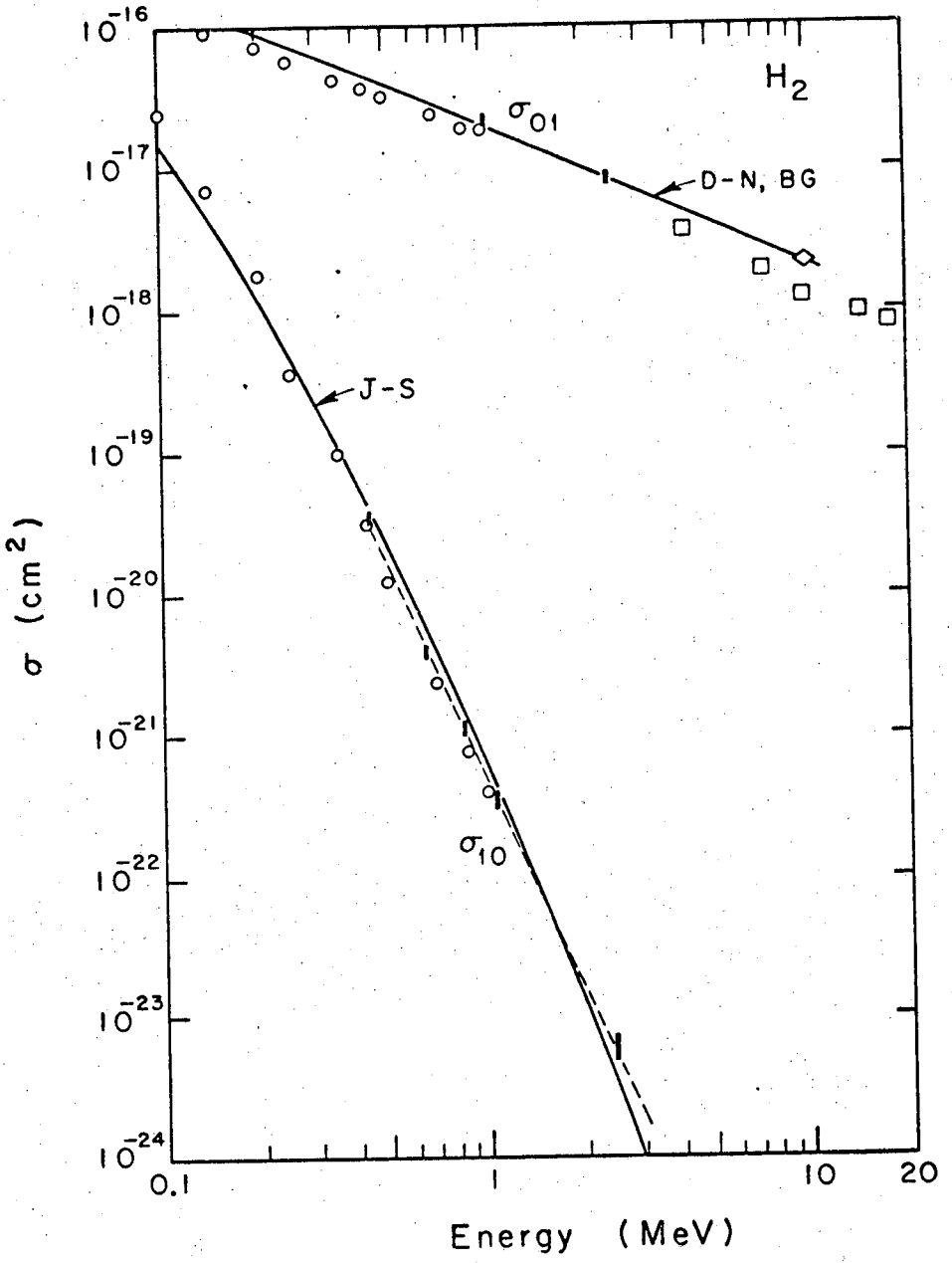

Fig. 5. H_2 results. Present results indicated by solid bar ▌. Symbols used: Experimental results: o, Barnett and Reynolds (Ref. 11); ◇, Berkner et al. (Ref. 51); □, Smythe and Toevs (Ref. 53). Theoretical results: D-N, Dmitriev and Nikolaev (Ref. 47); B-5, Bates and Griffing (Ref. 48); J-S, Jackson and Schiff (Ref. 22). Dashed line is drawn through the present results.

The calculation, done for atomic hydrogen, has been multiplied by 2 for the comparison with molecular hydrogen results. The accuracy of this approximation is a subject of discussion in Sections II and VI.

The curve plotted is for capture into all states, assuming that capture into excited states is proportional to $1/n^3$. [22]

The results for σ_{01}, both for H_2 and He, fit well with the predictions of Dmitriev and Nikolaev,[47] Bates and Griffing,[48] and Bates and Williams.[49]

2. Helium Gas, He

σ_{10} (cm^2/mol)	Proton energy (MeV)
$1.6^3 \pm 0.16 \times 10^{-19}$	0.440 ± 0.003
$2.9^4 \pm 0.3 \times 10^{-20}$	0.654 ± 0.003
$8.3^4 \pm 0.8 \times 10^{-21}$	0.851 ± 0.004
$2.8^6 \pm 0.3 \times 10^{-21}$	1.063 ± 0.006
$3.1^7 \pm 0.3 \times 10^{-23}$	2.45 ± 0.03
$1.2^1 \pm 0.1 \times 10^{-23}$	2.99 ± 0.04
$5.3^5 \pm 0.5 \times 10^{-25}$	5.41 ± 0.05

σ_{01} (cm^2/mol)	H^0 energy (MeV)
$1.4^8 \pm 0.1 \times 10^{-17}$	1.027 ± 0.006
$6.3^2 \pm 0.5 \times 10^{-18}$	2.44 ± 0.03

These results are plotted in Fig. 6. The dashed line drawn through the present results has a behavior of $\approx E^{5.3 \pm 0.1}$ at the high-energy end. The predictions of Bransden and Cheshire,[14] of R. A. Mapleton,[33] and of Mittleman,[15] as evaluated by Berkner et al.,[13] are also shown.

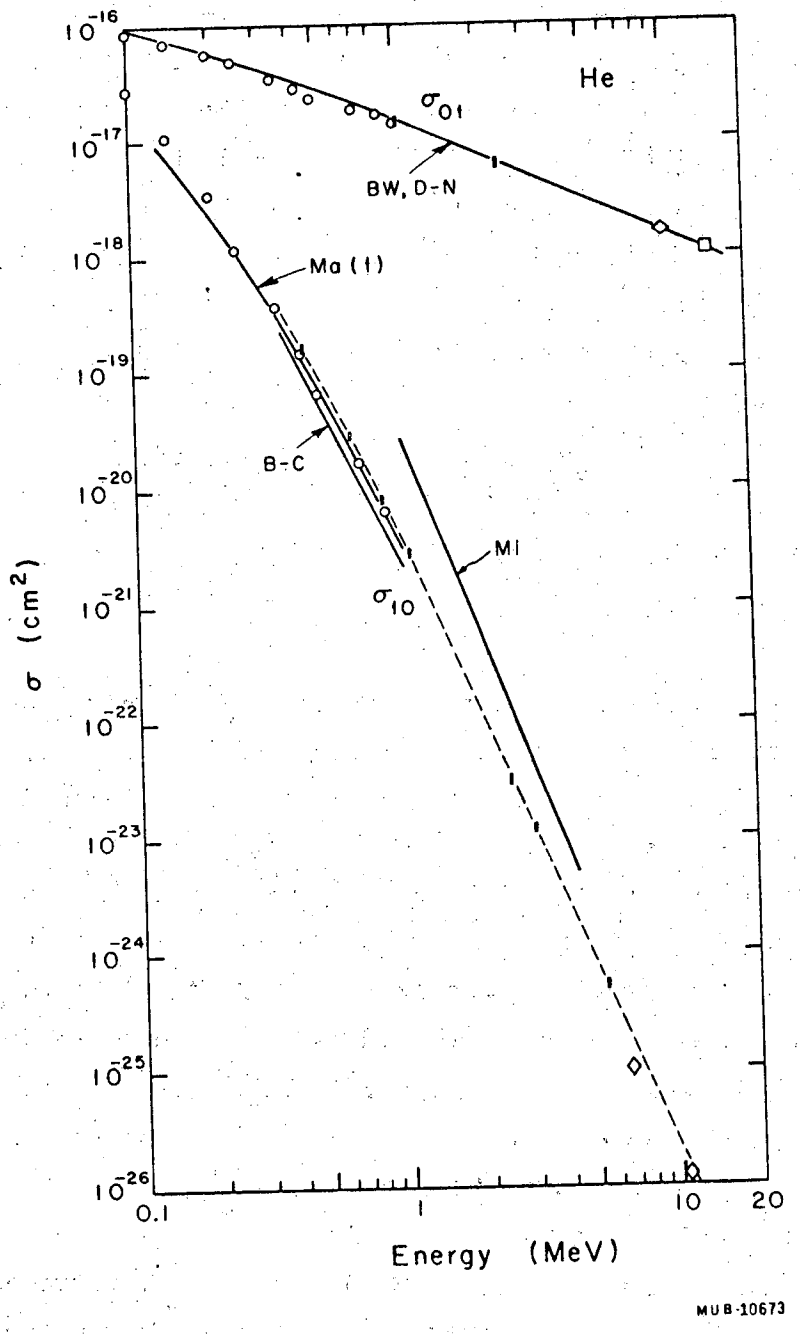

Fig. 6. He results. Present results indicated by solid bar, ▮. Other symbols: Experimental results; O, Barnett and Reynolds (Ref. 11); ◇, Berkner et al. (Ref. 51); □, Smythe and Toevs (Ref. 53); ◊, Berkner et al. (Ref. 13). Theoretical results: B-W, Bates and Williams (Ref. 49); D-N, Dmitriev and Nikolaev (Ref. 47); B-C, Bransden and Cheshire (Ref. 14); Mi, Mittleman (Refs. 13 and 15); Ma (1), Mapleton (Ref. 33). Dashed line is drawn through the present results.

3. Nitrogen Gas, N_2

σ_{10} (cm^2/mol)	Proton energy (MeV)
$9.7^9 \pm 0.9 \times 10^{-19}$	0.440 ± 0.003
$2.4^8 \pm 0.3 \times 10^{-19}$	0.654 ± 0.003
$9.8^1 \pm 0.9 \times 10^{-20}$	0.851 ± 0.004
$5.1^4 \pm 0.5 \times 10^{-20}$	1.063 ± 0.006
$2.0^6 \pm 0.2 \times 10^{-21}$	2.51 ± 0.03
$1.4^0 \pm 0.15 \times 10^{-22}$	4.79 ± 0.05
$9.8^5 \pm 0.9 \times 10^{-25}$	13.75 ± 0.2

σ_{01} (cm^2/mol)	H^0 energy (MeV)
$1.6^8 \pm 0.1 \times 10^{-16}$	1.027 ± 0.006
$7.2^2 \pm 0.6 \times 10^{-17}$	2.44 ± 0.03

Figure 7 shows plots of these points, plus other experimental measurements and the theoretical predictions of Mapleton,[32,34] and the evaluation of the first Born approximation by Mittleman.[13,15] Note that the present results reproduce the shape of a curve through the Barnett-Reynolds results, although they are larger by some 40%. The curve marked Ma (2) is for capture of p-orbital electrons in atomic nitrogen into the 1s state of hydrogen, estimating the Born "full-interaction potential" cross section as discussed in Section II D. The curve marked Ma (3) is the OBK calculation for p-orbital capture from which Ma (2) was obtained, but adjusted to include capture into all states. The curve marked Ma (4) is the result of the OBK calculation above 1 MeV, including 1s- and 2s-orbital capture also.[50]

As with hydrogen, the calculations for atomic nitrogen have been multiplied by 2 as an approximation to the case for capture from molecular nitrogen.

The dotted section of the Mi curve is simply an extension below the expected range of validity of the calculation in order to show more clearly the relative slope of the curve (E^{-6}).

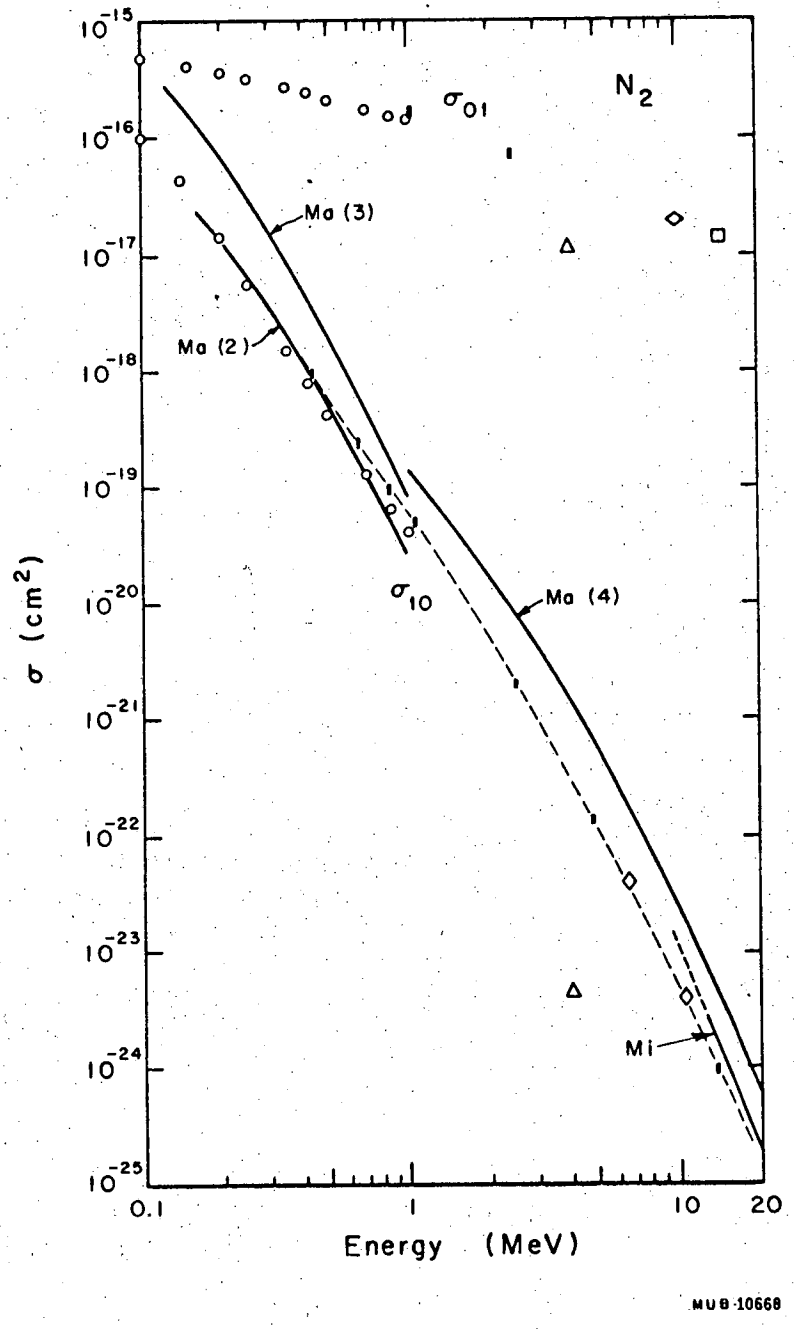

Fig. 7. N_2 results. Present results indicated by solid bar, ▌. Other symbols: Experimental results: o, Barnett and Reynolds (Ref. 11); ◇, Berkner et al. (Ref. 51); □, Smythe and Toevs (Ref. 53); △, Szostak et al. (Ref. 12); ◊, Berkner et al. (Ref. 13). Theoretical results: Ma (2), Ma (3), Mapleton (Ref. 32); Ma (4), Mapleton (Ref. 34); Mi, Mittleman (Refs. 13 and 15). Dashed line is drawn through the present results.

4. Argon Gas, Ar

σ_{10} (cm^2/mol)	Proton energy (MeV)
$5.8^0 \pm 0.5 \times 10^{-19}$	0.440 ± 0.003
$2.6^7 \pm 0.3 \times 10^{-19}$	0.654 ± 0.003
$1.5^1 \pm 0.15 \times 10^{-19}$	0.851 ± 0.004
$8.8^9 \pm 0.8 \times 10^{-20}$	1.063 ± 0.006
$4.2^6 \pm 0.4 \times 10^{-21}$	2.51 ± 0.03
$3.2^4 \pm 0.3 \times 10^{-22}$	4.79 ± 0.05
$5.4^6 \pm 0.5 \times 10^{-24}$	13.75 ± 0.2

σ_{01} (cm^2/mol)	H^0 energy (MeV)
$1.7^6 \pm 0.15 \times 10^{-16}$	1.027 ± 0.006
$8.9^0 \pm 0.7 \times 10^{-17}$	2.44 ± 0.03

The above results are shown in Fig. 8. There are no known theoretical treatments for this case. Here, as in the N_2 case, we reproduce the shape of the σ_{10} curve of Barnett and Reynolds in the region of overlap, but with cross sections roughly 50% higher.

B. Error Analysis

The major sources of error in the measurement of σ_{10} are uncertainty in target gas pressure; neutral background counts, n_{b0}; impurities; and the correction due to electron loss in the target gas cell.

A detailed discussion of the effect of these and other uncertainties on σ_{10}, plus an error analysis for the measurements made of σ_{01}, are found in the Appendix.

In most cases, the total error in the value of specific cross sections is slightly less than 10%.

The errors associated with the measurement of proton energy, which are important because of the steep slope of the σ_{10} curves at high

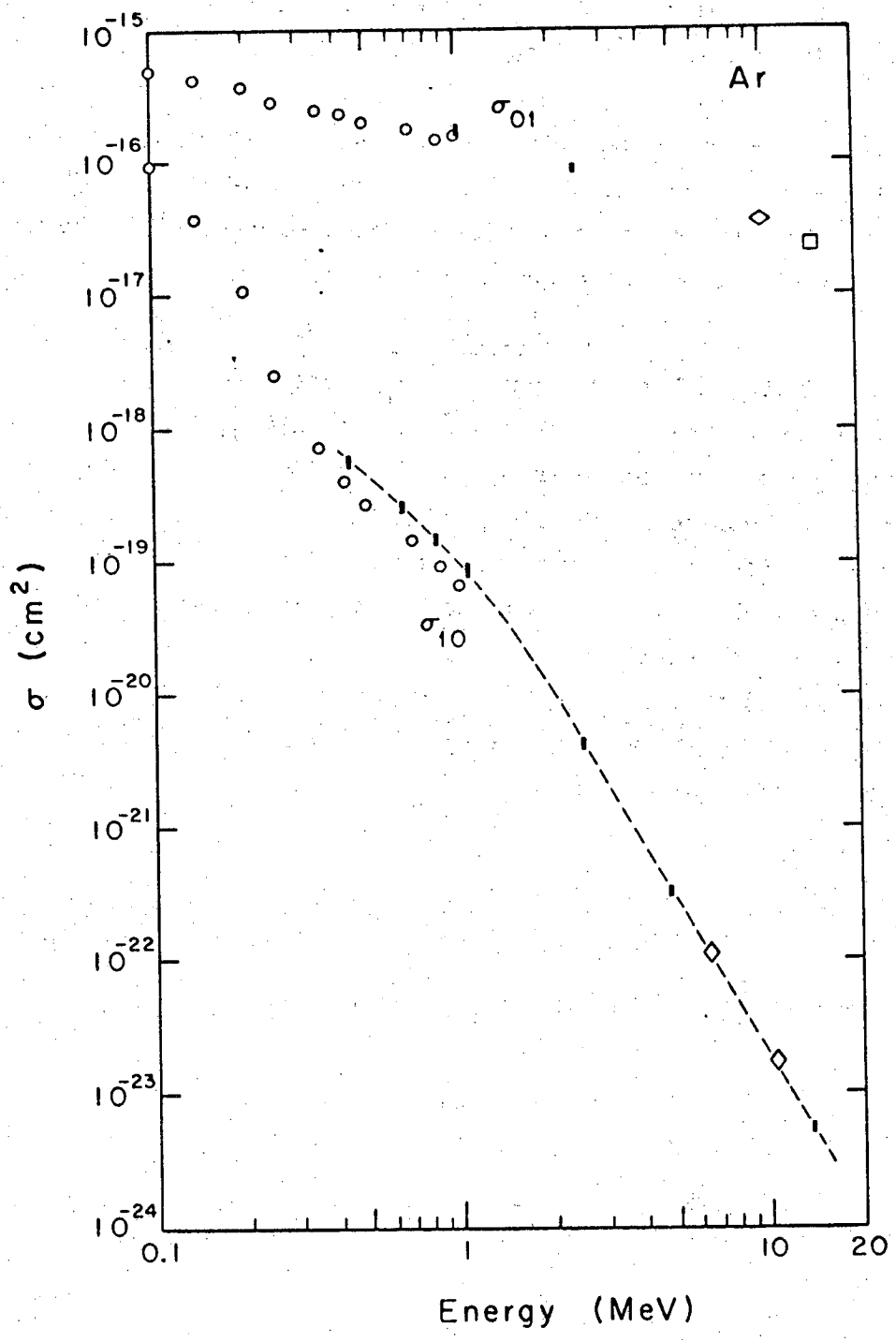

Fig. 8. Ar results. Present results indicated by solid bar, ▮. Other symbols: o, Barnett and Reynolds (Ref. 11); ◇, Berkner et al. (Ref. 51); □, Smythe and Toevs (Ref. 53); ◊, Berkner et al. (Ref. 13). Dashed line is drawn through the present results.

energies, have been discussed in Section III C.

It should be noted that wherever these σ_{10} results are to be compared with a calculation at a specified energy, the error associated with the energy measurement should then be accounted for in the error of the σ_{10} value used. If the σ_{10} curve has a slope of E^{-m} at the specified energy, the error $\Delta\sigma_{10}$ associated with the error ΔE of the energy measurement is approximately $\Delta\sigma_{10} \approx m\Delta E$.

C. Consistency of Measurements

Individual measurements of σ_{10} were made over a wide range of pressures. They were thus subject to varying errors, but generally did not change with pressure, as they would have if our pressure calibration, corrections for electron loss collisions, or measurement of neutral background counts were much in error. Figures 9 and 10 show, respectively, plots of data with error bars for a point (N_2 at 0.851 MeV) typical of the great majority of points, and for a point (H_2 at 0.654 MeV) with high n_{b0} (neutral background) and high associated errors. In both cases, the quoted result is plotted on the y axis (i.e., at 0 pressure).

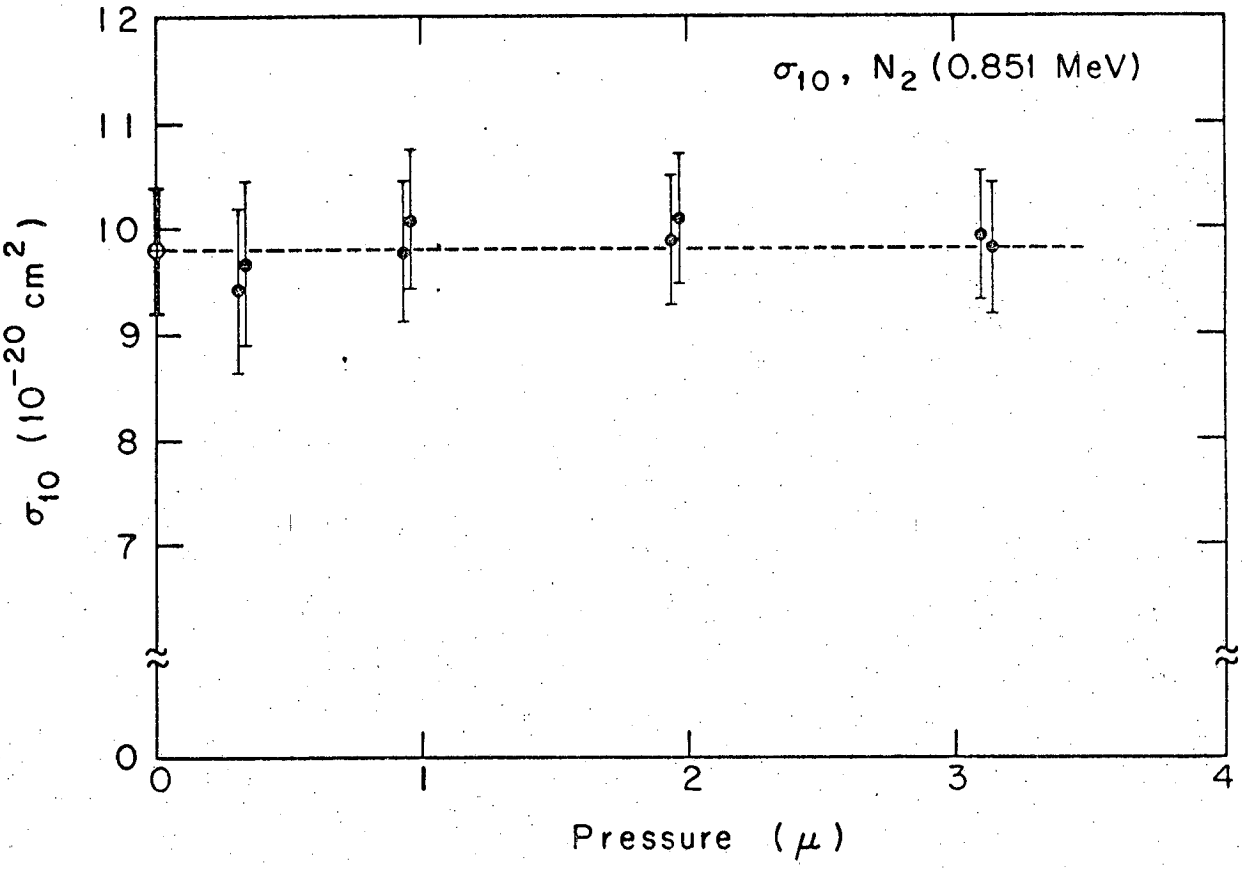

Fig. 9. Plot of individual measurements and probable errors for σ_{10} in N_2 at 0.851 MeV.

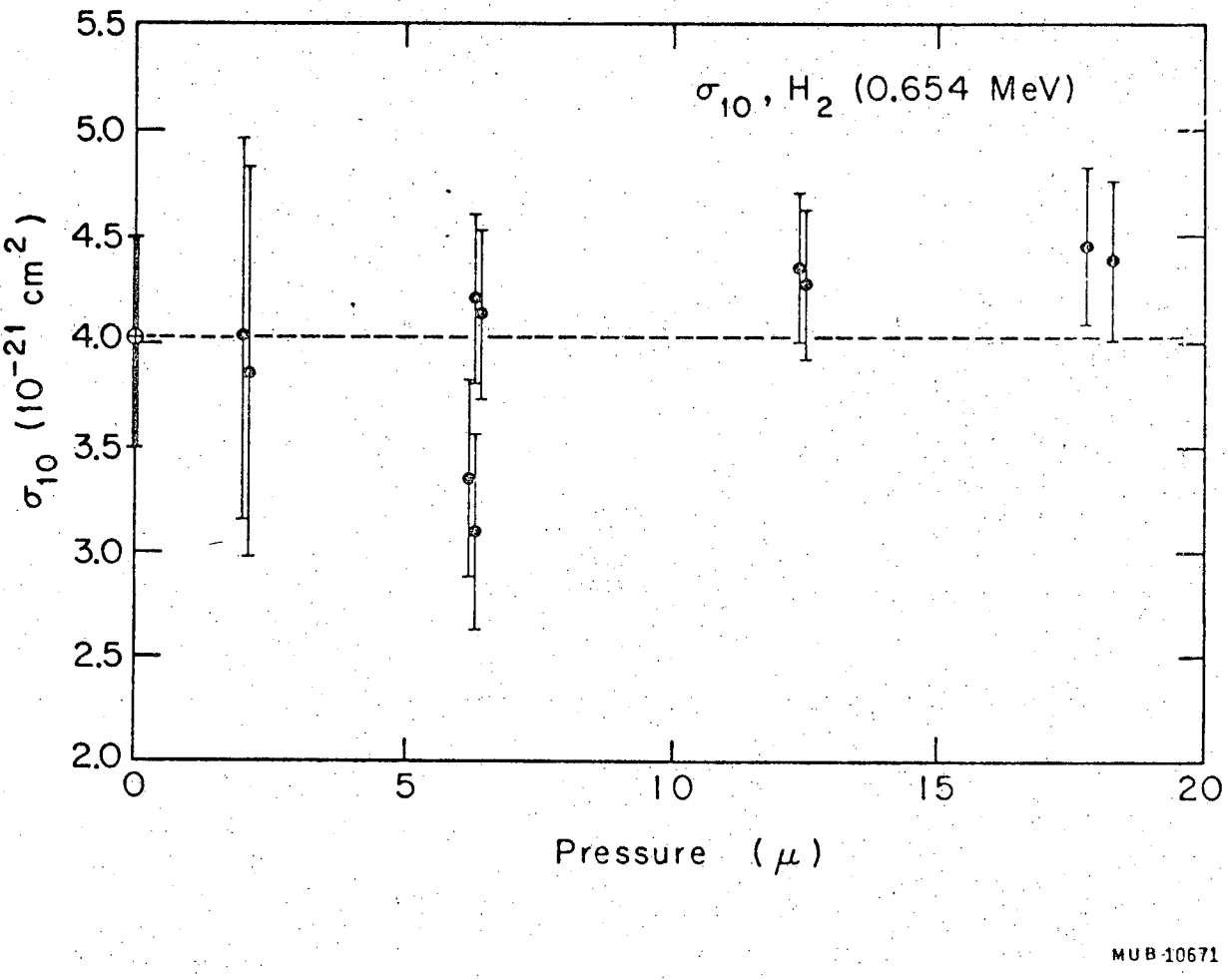

Fig. 10. Plot of individual measurements and probable errors for σ_{10} in H_2 at 0.654 MeV.

VI. SUMMARY AND CONCLUSIONS

There are several comments apropos to the measurements in specific gases, so the results are first discussed individually.

A. H_2

There is agreement between our results in H_2 and those of Barnett and Reynolds, within experimental error. We were able to extend this measurement only to 2.45 MeV, primarily because of increasingly difficult neutral background count problems at higher energies. This new information, however, is interesting in regard to the work of Tuan and Gerjuoy,[35] which involves the relationship between σ_{10} for atomic hydrogen and σ_{10} for molecular hydrogen. Calculations for capture from hydrogen have been done for atomic hydrogen almost exclusively, and comparison with experimental results in H_2 has been made by doubling the calculated atomic cross sections. The general thesis of Tuan and Gerjuoy is that for energies just above 400 keV, σ_{10} (molecular) is actually less than twice σ_{10} (atomic), but that in the high energy limit σ_{10} (molecular) is 2.4 to 2.8 times σ_{10} (atomic). As is seen in Fig. 5, the specific data we present appear to behave similarly relative to the Jackson-Schiff calculation. Since there is but one measurement above 1 MeV, the evidence is not conclusive. The result, however, does encourage additional measurements, extending to higher energies, to confirm or disprove this apparent crossover.

B. He

In helium also there is good agreement between our results and those of Barnett and Reynolds. There appears to be close agreement between Mapleton's first Born calculation, plotted in Fig. 6 for capture into the ground state of hydrogen only, and the experimental results. The slope of the σ_{10} curve in He appears to be changing very slowly if at all at high energies, i.e., up to approximately 10 MeV. There are possible corrections to the data of Berkner et al.,[51] which would raise their points some 25 to 30%,[52] near but still below the straight line through the present results. This gas probably offers

the best chance of experimentally determining a limiting high-energy behavior for comparison with the results of nonrelativistic calculations. The "high energy" limit is expected at lower proton energies than for other gases than hydrogen, and helium does not present the complication of a diatomic molecule. In spite of the apparent straight-line behavior of the results above 1 MeV, a measurement of σ_{10} at an energy substantially above 10 MeV appears necessary before one could claim to have shown an asymptotic limit experimentally.

C. N_2

The similar curvatures found in the experimental results here and by Barnett and Reynolds suggest that there is some structure to the σ_{10} curve for N_2 below 1 MeV. The structure seems to be qualitatively explained by comparison to the curves of Oppenheimer-Brinkman-Kramers σ_{10}, by Mapleton,[32,34] plotted on Fig. 7 as Ma (3) and Ma (4). Ma (3) includes capture of p-orbital electrons of atomic nitrogen only, since at lower energies p-orbital capture dominates capture from s states. Ma (4) includes both p- and s-orbital capture; capture from s states dominates at high energies. From these curves it seems apparent that the complete σ_{10} OBK calculation would show a shape similar to that observed experimentally. The suggestion is that the observed changes in curvature of the σ_{10} curve may be attributable to differing dominant capture reactions at different energies. Capture of p electrons falls off as E^{-6}.[32]

There is a disparity between the experimental results of Barnett and Reynolds and ours of about 40%, which is beyond that expected from the quoted errors. We have been able to find no explanation for this.

D. Ar

In argon also our results are greater by some 50% than those of Barnett and Reynolds, still without easy explanation. The matching shapes of the two resulting σ_{10} curves confirm a structure similar to but more pronounced than that in N_2, and in the same energy range.

E. Comments on Future Experiments

The results obtained in the work indicate a desirability of extending the measurements to higher energies, at least in hydrogen and helium. The experimental experience has pointed out some of the difficulties of doing this. The problem of too large a background neutral count increases with energy, as the electron-capture cross sections of the light gases fall off much more rapidly than those of the background gas constituents. To reduce the importance of background neutrals, further experiments should provide for sweeping magnets before and after the gas target in order to determine accurately the sources of background counts.

Since there is certainly a practical limit to how much one can reduce background gas pressure and drift lengths, the experimenter may find it advantageous to use a thicker gas target, even to the point where the beam components come to equilibrium. This will add the full uncertainty of the σ_{01} value at that energy to the probable error of the measurements, but it will both raise the proportion of "true" counts and limit the drift length of concern to that after the gas target. Spread of the beam from multiple collisions should not be insurmountable.

ACKNOWLEDGMENTS

I wish to thank very much Dr. Robert V. Pyle for his active interest and guidance, and Dr. C. M. Van Atta for his support of this research. Many thanks are due also to Dr. Klaus H. Berkner and Dr. Selig N. Kaplan for their generous participation in the experiments, to J. Warren Stearns, Vincent J. Honey, and John C. Warren for their assistance in assembling and operating the equipment, and to Margaret R. Thomas for her very real help in typing the manuscript.

This work was performed under the auspices of the U. S. Atomic Energy Commission.

APPENDIX

Error Analysis

We wish to estimate the standard deviation in σ_{10} resulting from uncertainty in (1) target thickness, Π; (2) knowledge of the electron loss cross section σ_{01}; (3) total particle counts, N_0 and N_+; (4) total background counts, n_{b0}; (5) the relative fractions of total neutral background counts originating before and after the target, n_{b1} and n_{b2}; and (6) the effect of impurities. We will find it convenient to expand the formula for σ_{10} to get

$$\sigma_{10} = \frac{N_0 - n_{b2} - n_{b1} e^{-\Pi\sigma_{01}}}{N_+ \Pi \left[1 - \frac{\Pi\sigma_{01}}{2} + \frac{\Pi^2 \sigma_{01}^{\ 2}}{6} - \frac{\Pi^3 \sigma_{01}^{\ 3}}{24} + \cdots \right]} .$$

The series $1 - \Pi\sigma_{01}/2 + \Pi^2\sigma_{01}^{\ 2}/6 - \Pi^3\sigma_{01}^{\ 3}/24 + \cdots$ differs from $e^{-\Pi\sigma_{01}/2}$ by no more than 1% over our range of $\Pi\sigma_{01}$, so we will henceforth use this approximate equivalence. The σ_{10} formula can then be written as

$$\sigma_{10} = \frac{N_0 \left[1 - (1 - f)K - fKe^{-\Pi\sigma_{01}} \right]}{N_+ \Pi e^{-\Pi\sigma_{01}/2}},$$

where

$K = \frac{n_{b0}}{N_0}$, the ratio of total background counts to total neutral counts,

and

$f = \frac{n_{b1}}{n_{b0}}$, the fraction of background originating before the target.

1. Target Thickness Π

Differentiating with respect to Π, we find

$$\frac{\partial\sigma_{10}}{\sigma_{10}} = -\frac{\partial\Pi}{\Pi}\left[1 - \frac{\Pi\sigma_{01}}{2}\,\frac{1 - (1 - f)K + fKe^{-\Pi\sigma_{01}}}{1 - (1 - f)K - fKe^{-\Pi\sigma_{01}}}\right].$$

We have estimated f to be 0.8. To help in seeing the behavior of this function, we have plotted, in Fig. 11, $(-\Delta\sigma_{10}/\sigma_{10})/(\Delta\Pi/\Pi)$ vs. $\Pi\sigma_{01}$ over the ranges used in our measurements. The dotted lines connect the individual measurements made for the indicated target gas and proton beam energy. The points shown are typical of those with high relative background. Most of the data taken lie between K = 0 and K = 0.2.

Uncertainty in knowledge of target thickness arises from the previously discussed error in pressure calibration and from uncertainty in the effective target length (e.g., pressure distribution in collimators, particle distribution in the differential pumping section), which is estimated at ± 2%.

The error, then, in σ_{10} due to Π ranges from ± 8% for most points in N_2 and Ar down to ± 4% for the 2.45-MeV point in H_2.

2. Electron-Loss Cross Section, σ_{01}

$$\frac{\partial\sigma_{10}}{\sigma_{10}} = \frac{\partial\sigma_{01}}{\sigma_{01}}\left[\frac{\Pi\sigma_{01}}{2}\,\frac{1 - (1 - f)K + fKe^{-\Pi\sigma_{01}}}{1 - (1 - f)K - fKe^{-\Pi\sigma_{01}}}\right].$$

The function $(\Delta\sigma_{10}/\sigma_{10})/(\Delta\sigma_{01}/\sigma_{01})$ is also plotted in Fig. 11, with the ordinate values shown on the right side of the figure. Considering the error in the values of σ_{01} used in the calculation to be ± 10%, we see that the error induced in σ_{10} varies from ≈ 2% for most cases to ≈ 5% in H_2 at 2.45 MeV.

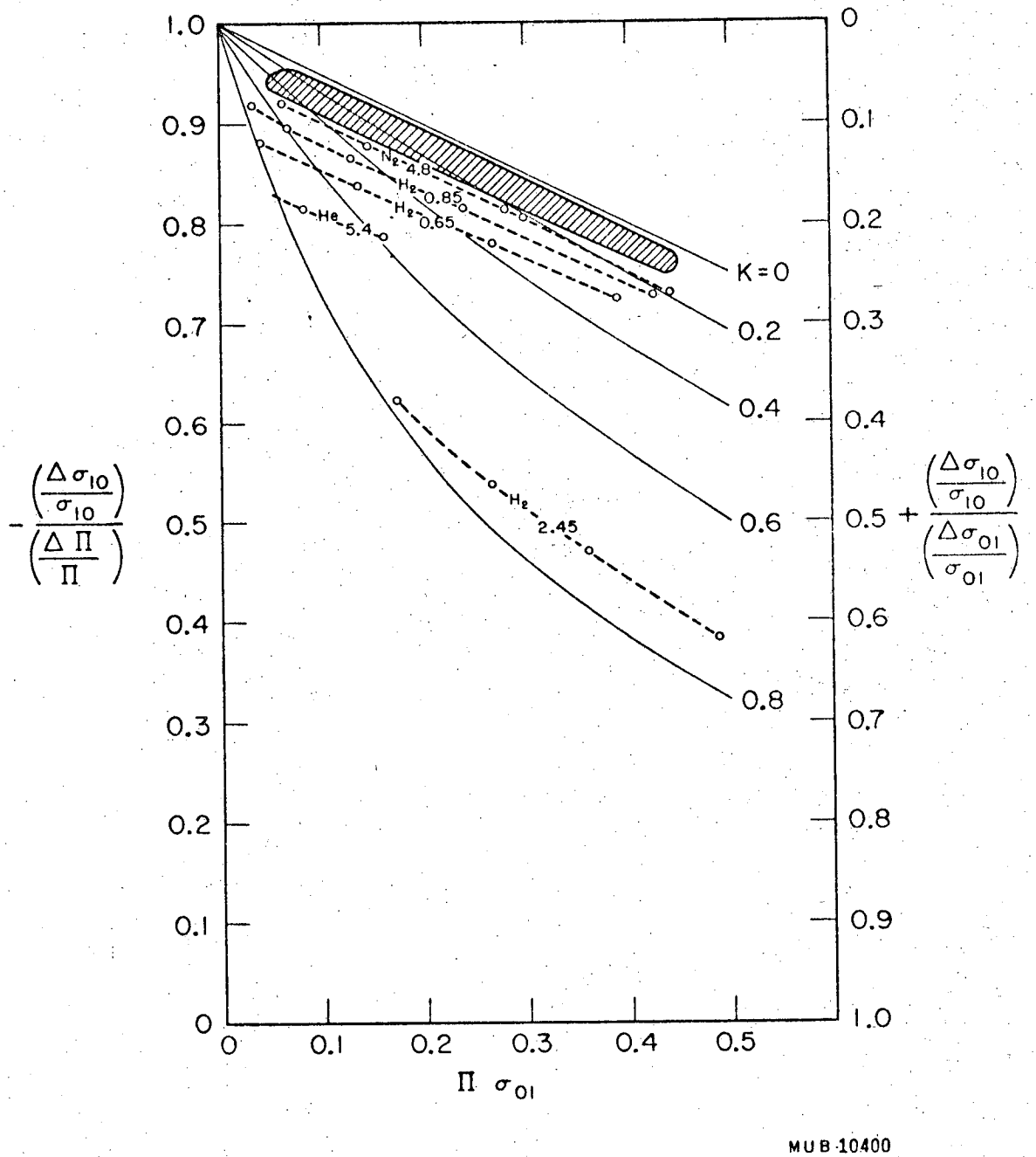

Fig. 11 Plot of error in σ_{10} resulting from uncertainty in target thickness Π (left-hand scale) and from uncertainty in value of σ_{01} (right-hand scale). Circles identify measurement points.

3. Total Particle Counts, N_0 and N_+

$$\frac{\partial\sigma_{10}}{\sigma_{10}} = \frac{\partial N_0}{N_0}\left[\frac{1}{1 - 0.2K - 0.8Ke^{-\Pi\sigma_{01}}}\right],$$

$$\frac{\partial\sigma_{10}}{\sigma_{10}} = -\frac{\partial N_+}{N_+}.$$

Counting errors for neutrals should be $\leqslant 1\%$. This error will have an appreciable effect only for measurements with high relative background, such as that for H_2 at 2.45 MeV, where $(\Delta\sigma_{10}/\sigma_{10})/(\Delta N_0/N_0)$ is significantly greater than 1. This is illustrated by Fig. 12, which shows $(\Delta\sigma_{10}/\sigma_{10})/(\Delta N_0/N_0)$ vs. $\Pi\sigma_{01}$, using the same parameters as in Fig. 11.

As discussed in Section III, the error in measurement of N_+ is $\pm$ 1.5%

4. Neutral Background Counts, n_{b0}

The dependence upon n_{b0} is

$$\frac{\partial\sigma_{10}}{\sigma_{10}} = -\frac{\partial n_{b0}}{n_{b0}}\left[\frac{1}{1 - 0.2K - 0.8Ke^{-\Pi\sigma_{01}}} - 1\right].$$

This function is plotted also on Fig. 12, with ordinate values shown on the right-hand scale. Measurements taken at lower pressures are subject to large errors from this source, since scatter in the n_{b0} measurements indicates a standard deviation in n_{b0} as high as 15% in a few cases.

5. Fraction of Neutral Background Originating Before Gas Target, f

Background neutrals may originate in background gas either before or after the target cell, or they may result from beam scraping on the collimators of the cell. Since estimates of the number created in the background gas account for virtually all observed, we have assumed

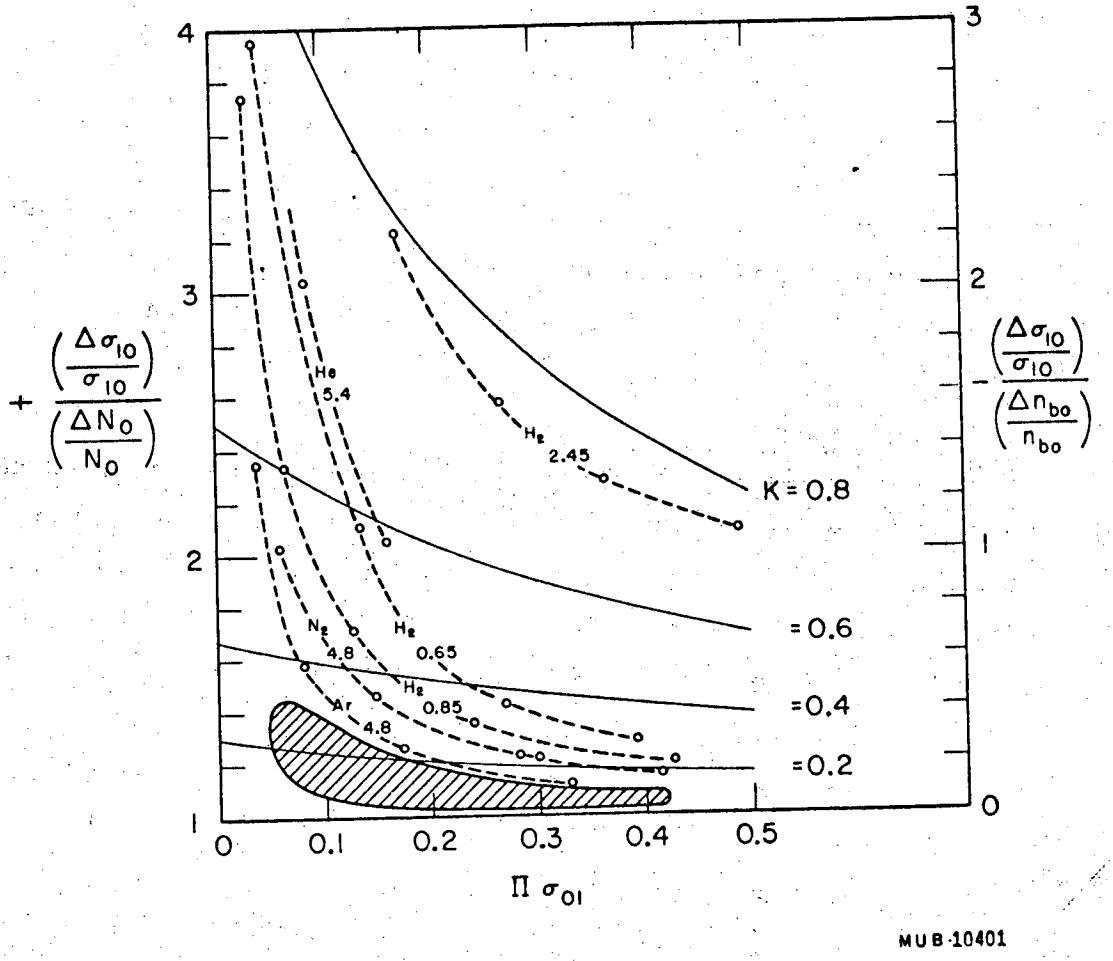

Fig. 12. Plot of error in σ_{10} resulting from uncertainty in total neutral count N_0 (left-hand scale) and in neutral background level (right-hand scale). Circles identify measurement points.

only a small fraction of n_{b0} to come from collimator scraping. Therefore f is determined largely from drift path lengths:

$$\frac{\partial\sigma_{10}}{\sigma_{10}} = \frac{\partial f}{f} \cdot \frac{fK\left[1 - e^{-\Pi\sigma_{01}}\right]}{1 - (1 - f)K - fKe^{-\Pi\sigma_{01}}} .$$

We estimate the figure f = 0.8 to be accurate to within about 10%. A 10% error there produces a significant error in only one of the measured points, σ_{10} for H_2 at 2.45 MeV, where the resulting error is ± 4%.

6. Impurities in H_2

The uncertainty in our knowledge of impurity concentrations and their capture cross sections for the H_2 gas used is about ± 30%. The magnitude of the correction itself varies with energy from 2% to 17%. Accordingly, the contribution to error in σ_{10} is between ± 0.6% and ± 5.1%, depending upon the energy of the particular measurement.

7. Total Error

The total error is found from the various error contributions by

$$\left(\frac{\Delta\sigma_{10}}{\sigma_{10}}\right)_{total} = \left[\sum_j \left(\frac{\Delta\sigma_{10}}{\sigma_{10}}\right)_j^2\right]^{1/2}, \text{ where } \left(\frac{\Delta\sigma_{10}}{\sigma_{10}}\right)_j \equiv \text{error from } j\text{th source.}$$

Although we take the mean of many measurements for each point, thus reducing statistical inaccuracies such as occur in, say, measuring n_{b0}, the total error is not significantly reduced, since it includes an estimate of the probability of systematic errors, as in target thickness Π, which remain unaffected by the number of measurements made.

Error Analysis, σ_{01}

With $$\sigma_{01} = \frac{1}{\Pi} \ln\left[1 + \frac{N_+ - n_{b+}}{N_0}\right]$$

we see immediately that

$$\frac{\Delta\sigma_{01}}{\sigma_{01}} = \frac{-\Delta\Pi}{\Pi} .$$

Partial differentiation with respect to the counting variables results in

$$\frac{\partial\sigma_{01}}{\sigma_{01}} = \frac{\partial N_+}{N_+} \frac{N_+/N_0}{\left[1 + \frac{N_+ - n_{b+}}{N_0}\right] \ln\left[1 + \frac{N_+ - n_{b+}}{N_0}\right]},$$

$$\frac{\partial\sigma_{01}}{\sigma_{01}} = -\frac{\partial n_{b+}}{n_{b+}} \frac{n_{b+}/N_0}{\left[1 + \frac{N_+ - n_{b+}}{N_0}\right] \ln\left[1 + \frac{N_+ - n_{b+}}{N_0}\right]},$$

$$\frac{\partial\sigma_{01}}{\sigma_{01}} = -\frac{\partial N_0}{N_0} \frac{(N_+ - n_{b+})/N_0}{\left[1 + \frac{N_+ - n_{b+}}{N_0}\right] \ln\left[1 + \frac{N_+ - n_{b+}}{N_0}\right]} .$$

The multiplying factors on the right sides of the above three equations are of order one or smaller in all cases. Counting errors are thus considered to be, here also, relatively unimportant.

We estimate the deviation of the σ_{01} measurements to be no more than 10% for all cases.

FOOTNOTES AND REFERENCES

1. L. H. Thomas, On the Capture of Electrons by Swiftly Moving Electrified Particles, Proc. Roy. Soc. (London) A114, 561 (1927).
2. H. C. Brinkman and H. A. Kramers, Zur Theorie der Einfangung von Elektronen durch α-Teilchen, Proc. Acad. Sci. Amsterdam 33, 973 (1930).
3. F. L. Ribe, Electron-Capture Cross Sections for Protons Passing through Hydrogen Gas, Phys. Rev. 83, 1217 (1951).
4. Ya. M. Fogel, L. I. Krupnik, and B. G. Safranov, Capture of Electrons and Ionization by Protons in Hydrogen, Soviet Phys.-JETP 1, 415 (1955).
5. J. B. H. Stedeford and J. B. Hasted, Further Investigations of Charge Exchange and Electron Detachment, Proc. Roy. Soc. (London) A227, 466 (1955).
6. H. B. Gilbody and J. B. Hasted, Anomolies in the Adiabatic Interpretation of Charge-Transfer Collisions, Proc. Roy. Soc. (London) A238, 334 (1956).
7. V. V. Afrosimov, R. N. Il'in, and N. V. Fedorenko, The Ionization of Argon by Hydrogen Ions, Soviet Phys.-J. Tech. Phys. 3, 2080 (1958).
8. R. N. Il'in, V. V. Afrosimov, and N. V. Fedorenko, Ionization of Air by H^+ and H_2^+ Ions, Soviet Phys.-JETP 9, 29 (1959).
9. V. V. Afrosimov, R. N. Il'in, and N. V. Fedorenko, Ionization of Molecular Hydrogen by H^+, H_2^+, and H_3^+ Ions, Soviet Phys.-JETP 7, 968 (1958).
10. P. M. Stier and C. F. Barnett, Charge Exchange Cross Sections of Hydrogen Ions in Gases, Phys. Rev. 103, 896 (1956).
11. C. F. Barnett and H. K. Reynolds, Charge Exchange Cross Sections of Hydrogen Particles in Gases at High Energies, Phys. Rev. 109, 355 (1958).
12. R. Szostak, M. Martin, and P. Marmier, Umladung von Protonen bei 4 MeV in Stickstoff, Helv. Phys. Acta 34, 485 (1961).

13. Klaus H. Berkner, Selig N. Kaplan, George A. Paulikas, and Robert V. Pyle, Electron Capture by High-Energy Deuterons in Gases, Phys. Rev. 140, A729 (1965).

14. B. H. Bransden and I. M. Cheshire, Electron Capture from Helium by Fast Protons, Proc. Phys. Soc. (London) 81, 820 (1963).

15. M. H. Mittleman, Rearrangement Collisions III. Electron Transfer from Atoms to Fast Protons, Proc. Phys. Soc. (London) 81, 633 (1963).

16. D. R. Bates and R. McCarroll, Charge Transfer, Advances in Phys. 11, 39 (1962).

17. N. F. Mott and H. S. W. Massey, The Theory of Atomic Collisions, Third Edition (Oxford University Press, London, 1965), p. 618.

18. C. J. Cook, The Asymptotic Form of the Electron Capture Cross Sections, Proc. Phys. Soc. (London) 81, 789 (1963).

19. Michal Gryzinski, Classical Theory of Atomic Collisions I. Theory of Inelastic Collisions, Phys. Rev. 138, A336 (1965).

20. D. R. Bates and R. A. Mapleton, Classical Calculations on Electron Capture, Proc. Phys. Soc. (London) 87, 657 (1966).

21. J. R. Oppenheimer, On the Quantum Theory of the Capture of Electrons, Phys. Rev. 31, 349 (1928).

22. J. David Jackson and Harry Schiff, Electron Capture by Protons Passing through Hydrogen, Phys. Rev. 89, 359 (1953).

23. Richard M. Drisko, The Theories of Positronium and of Rearrangement Collisions (Thesis), Carnegie Institute of Technology, 1955 (unpublished). See references 15 and 26.

24. Ronald Aaron, Ralph D. Amado, and Benjamin W. Lee, Divergence of the Green's Function Series for Rearrangement Collisions, Phys. Rev. 121, 319 (1961).

25. Marvin H. Mittleman, Proton-Hydrogen Scattering System, Phys. Rev. 122, 499 (1961).

26. R. H. Bassel and E. Gerjuoy, Distorted Wave Method for Electron Capture from Atomic Hydrogen, Phys. Rev. 117, 749 (1960).

27. I. M. Cheshire, Continuum Distorted Wave Approximation; Resonant Charge Transfer by Fast Protons in Atomic Hydrogen, Proc. Phys. Soc. (London) 84, 89 (1964).

28. Trilochan Pradhan, Electron Capture by Protons Passing through Hydrogen, Phys. Rev. 105, 1250 (1957).

29. I. M. Cheshire, Electron Capture by Fast Protons in Hydrogen, Proc. Phys. Soc. (London) 82, 113 (1963).

30. The Z dependence as originally given in reference 15 is incorrect; M. H. Mittleman, Space Sciences Laboratory, University of California, Berkeley, private communication.

31. Robert A. Mapleton, Electron Capture from Atomic Hydrogen by Protons, Phys. Rev. 126, 1477 (1962).

32. Robert A. Mapleton, Electron Capture from Atomic Nitrogen and Oxygen by Protons, I, Phys. Rev. 130, 1829 (1963).

33. Robert A. Mapleton, Electron Capture from He ($1s^2$) by Protons, II, Phys. Rev. 130, 1839 (1963).

34. Robert A. Mapleton, Electron Capture from Atomic Nitrogen by Protons, Phys. Rev. 145, 25 (1966).

35. T. F. Tuan and E. Gerjuoy, Charge Transfer in Molecular Hydrogen, Phys. Rev. 117, 756 (1960).

36. Kazem Omidvar, Electron Capture by Protons in Hydrogen in an Electric Field, Goddard Space Flight Center Report X-641-65-306, July 1965 (unpublished).

37. S. K. Allison and M. Garcia-Munoz, Electron Capture and Loss at High Energies, in Atomic and Molecular Processes, edited by D. R. Bates (Academic Press, New York and London, 1962), p. 749.

38. Hiroshi Ishii and Katsuya Nakayama, A Serious Error Caused by Mercury Vapor Stream in the Measurement with a McLeod Gauge in the Cold Trap System (Effect of the Diffusion of Nitrogen in the Mercury Vapour Stream), in Vacuum Symposium Transactions, Vol. I (Pergamon Press, New York and London, 1961), p. 519.

39. Ch. Meinke and G. Reich, Influence of Diffusion on the Measurement of Low Pressure with the McLeod Vacuum Gauge, Vacuum 13, 579 (1963).

40. J. H. Leck, Pressure Measurement in Vacuum Systems (The Institute of Physics, London, 1957), p. 16.

41. A. B. Wittkower, P. H. Rose; R. P. Bastide, and N. B. Brooks, Small-angle Scattering Observed in the Formation of Neutral Atoms from 10- to 55-keV Positive Ion Beams, Phys. Rev. 136, A1254 (1964).

42. R. McCarroll, Resonance Charge Transfer between H(1s) and H^+ Calculated by Means of an Approximation Based on an Expansion in Atomic Eigenfunctions, Proc. Roy. Soc. (London) A264, 547 (1961).

43. V. J. Ashby and M. A. Williamson; revised by Rex Booth, Cyclotron Range-Energy Measurement Instructions, Lawrence Radiation Laboratory, Livermore, Physics Division Report, Nuc. Phys. 123, Rev. 1, April 20, 1959 (unpublished).

44. Jerry B. Marion, Accelerator Energy Calibrations, Rev. Mod. Phys. 33, 139 (1961).

45. W. A. Aron, B. G. Hoffman, and F. C. Williams, Range Energy Curves, US AEC Report AECU-663, May 28, 1951.

46. Samuel K. Allison, Experimental Results on Charge-Changing Collisions of Hydrogen and Helium Atoms and Ions at Kinetic Energies above 0.2 keV, Rev. Mod. Phys. 30, 1137 (1958).

47. I. S. Dmitriev and V. S. Nikolaev, Calculation of the Cross Sections for Electron Loss by Fast Ions in Light Media, Soviet Phys.-JETP 17, 447 (1963).

48. D. R. Bates and G. W. Griffing, Inelastic Collisions between Heavy Particles. IV: Contribution of Double Transitions to Certain Cross Sections Including That Associated with the Ionization of Hydrogen Atoms in Fast Encounters with Other Hydrogen Atoms, Proc. Phys. Soc. (London) A68, 90 (1955).

49. D. R. Bates and A. Williams, Inelastic Collisions between Heavy Particles. VII: Electron Loss from Fast Hydrogen Atoms Passing through Helium, Proc. Phys. Soc. (London) A70, 306 (1957).

50. There are minor errors in the plot in reference 34, which are corrected in Ma (4). Robert A. Mapleton, Air Force Cambridge Research Laboratories, Bedford, Mass., private communication.

51. Klaus H. Berkner, Selig N. Kaplan, and Robert V. Pyle, Collisional Electron Detachment from 20-MeV D^0 and D^- Ions, Phys. Rev. 134, A1461 (1964).

52. Selig N. Kaplan, Lawrence Radiation Laboratory, University of California, Berkeley, private communication.

53. Rodman Smythe and James W. Toevs, Collisional Electron Detachment from Hydrogen Atoms and Negative Hydrogen between 4 and 18 MeV, Phys. Rev. 139, A15 (1965).